Burst Duration Representation of Timing: Modeling Coincidence Detection in Cerebellum-Like Granular Cells

Evan D. Vickers, Patrick D. Roberts, and Curtis C. Bell

(January 8, 2003)

Abstract

Gnathonemus petersii, a pulse-emitting African species of weakly electric fish, actively locates objects in its environment by measuring distortions of its own electric organ discharge that arrive at cutaneous electroreceptors (Bell, 1989). Current amplitude at these electroreceptors is neurally represented by the latencies of mormyromast afferent spikes. These latencies are transformed into a burst duration code by a corollary discharge gating mechanism (Szabo and Hagiwara, 1967) at the granular cell layer of the electrosensory lateral line lobe (ELL).

Mathematical models of stimulus intensity representation at the granular cell layer of ELL in the weakly electric fish, *Gnathonemus petersii,* were created to explore the biological mechanisms underlying a hypothesized neural code. The models are based on extracellular recordings from granular cells (Bell and Grant, 1992), intracellular recordings from afferent fibers electrotonically coupled to granular cells (Bell and Grant, 1992), and an earlier model of rat cerebellar granule cells (D'Angelo et al., 2001).

The models show that a persistent Na^+ current (I-NaP) and slow repolarizing K^+ current (I-KM) are sufficient to explain control of burst onset latency in granular cells. Offset latency is predicted to be controlled either by GABAergic inhibition from large multipolar interneurons (LMI) of the ELL or by variations in the activation kinetics of I-KM. It is shown that transformation of the latency code for stimulus intensity in afferent fibers to a burst duration code in the model granular cell is robust under moderate perturbations of synaptic inputs and ionic conductances.

KEY WORDS: electroreceptor afferents; electrosensory lateral line lobe (ELL); ELL granular cells; corollary discharge gating; burst duration code; latency-to-fire; persistent sodium current; slow potassium current

Abbreviated title: Stimulus representation in electric fish
Number of text pages: 21, number of figures: 15, number of tables: 2.
Number of words in abstract: 242 (250 words),
Number of words in the introduction: 499 (500 words),
Number of words in the discussion: 1439 (1500 words).
Corresponding author: Evan D. Vickers, Neurological Sciences Institute, OHSU, 505 N.W. 185th Avenue, Beaverton, OR 97006, e-mail: robertpa@ohsu.edu
Acknowledgments: This material is based upon work supported by the National Institutes of Health under Grant No. MH60364 to P.R. and Grant No. MH60996 to C.B., and the National Science Foundation under Grant No. IBN-0114558 to P.R.

Active electrolocation in *Gnathonemus petersi,* a pulse-emitting species of weakly electric fish, involves temporally precise neural mechanisms necessary for the detection of perturbations in electric field intensity. This stimulus intensity is initially coded as the latency to fire of mormyromast afferents (Szabo and Hagiwara, 1967). The timing of afferent inputs relative to an electric organ corollary discharge (EOCD) allows the fish to enhance only those signals likely to have been produced by distortions of its own electrical discharge (fig. 1; Bell, 1989).

Accurate representation of stimulus intensity requires a transformation from latency to burst duration coding at the granular cell layer of medial electrosensory lateral line lobe (ELL), which receives excitatory inputs from mormyromast afferents and the juxtalobar nucleus, and inhibitory inputs from large multipolar interneurons (LMI; fig. 2; Bell, 1989; Han et al., 2000). Because the small size of ELL granular cells (3-5 μm diameter) is prohibitive of patch clamping, mathematical modeling is currently the most efficient method of exploring the mechanisms underlying this transformation.

Two models, along with an earlier model constructed by D'Angelo et al. (2001), were used to test the hypothesis that the creation of a burst duration code from information about synaptic input delays relies on differential amplification of summed excitatory postsynaptic potentials (EPSPs) by a persistent sodium current (I-NaP). Primary afferent EPSPs arriving with post-EOCD delays brief enough to trigger granular cell spikes produce a graded response encoded as number of spikes in the granular cell burst following the arrival of each successive EOCD, as described by preliminary extracellular field recordings (fig. 3; Bell and Grant, 1992). Decreases in afferent latency, signaling increases in stimulus intensity, lengthen granular cell bursts (and *vice versa*).

Subthreshold voltage fluctuations can strongly influence the bursting properties of neurons (D'Angelo et al., 2001). In rat cerebellar granule cells these fluctuations are regular and periodic about resting membrane potential at frequencies of 3-12 Hz (D'Angelo et al., 2001). Resonance in this frequency range is driven primarily by a slow repolarizing K^+ current (I-KM) in combination with a persistent Na^+ current (I-NaP), as shown in D'Angelo's model. These two currents may be involved in differentially amplifying inputs to ELL granular cells and controlling burst duration via their subthreshold voltage effects.

The present study, in addition to making predictions concerning the role of intrinsic ionic conductances in the generation of an ELL granular cell burst duration representation of stimulus intensity, addresses the involvement of precisely timed inhibition in the refinement of this representation. This GABAergic inhibition, delivered by LMI projections onto granular cell somata, is known to be independent of Ca^{2+} and triggered by extracellular K^+ accumulation (Han et al., 2000). However, little is known about the temporal control of this inhibition in relation to stimulus encoding. The present models, along with recent work by Brand et al. (2002) showing that precisely timed inhibition is necessary for the coding of interaural time delays in mammals, support the idea that precisely timed inhibition, as a general principle, is crucial for submillisecond temporal resolution.

Methods

Two mathematical models of mormyrid ELL granular cell electroresponsiveness were constructed with NEURON v5.1 (Hines and Carnevale, 1997). The D'Angelo et al. (2001) model of the rat cerebellar granule cell was tested under constant current and synaptic input conditions to direct the development of models 1 and 2. Ion channel densities and synaptic currents in these models were then adjusted so that the voltage output matched the hypothesized transformation from afferent latency to granular cell burst duration. Model 1 included LMI inputs as a mechanism of burst termination, while model 2 relied entirely on intrinsic ion conductances.

Due to the electrotonically compact structure of ELL granular cells, models 1 and 2 were built as single compartment models (soma) with uniform ion conductance densities. Simulation of neuronal electrical properties was accomplished by numerically integrating a set of differential equations describing membrane voltage, intracellular Ca^{2+} concentration, and ion channel gating dynamics. Resting potential of the cell membrane was set to –65mV, and voltage changes were determined by the following equation:

$$-C_m \, dV/dt = \sum_i g_i \, (V-V_i) + I_{in} \qquad (1)$$

where V is membrane potential, t is time, C_m is membrane capacitance, g_i is ionic conductance, V_i is reversal potential of membrane conductance i, and I_{in} is injected current. Membrane conductances are represented using Hodgkin-Huxley-like models (Hodgkin and Huxley, 1952) of the type:

$$g_i = G_{max} \; x_i^{zi} \; y_i \qquad (2)$$

where G_{max} is the maximum ionic conductance, x_i and y_i are state variables (probabilities ranging from 0 to 1) for a gating variable, and z_i is the power of this gating variable in ion channel i. The variables x and y are related to the first-order rate constants α and β by the equations:

$$x_\infty = \alpha_x / (\alpha_x + \beta_x), \qquad y_\infty = \alpha_y / (\alpha_y + \beta_y) \qquad (3)$$
$$\tau_x = 1 / (\alpha_x + \beta_x), \qquad \tau_y = 1 / (\alpha_y + \beta_y) \qquad (4)$$

where α and β are functions of voltage. The equations used to parameterize α, β and the state variables x, τ_x, y, and τ_y for different ion channels (D'Angelo et al., 2001) are shown in Table 1. The state kinetic variables are:

$$dx/dt = (x_\infty - x) / \tau_x \qquad (5)$$
$$dy/dt = (y_\infty - y) / \tau_y \qquad (6)$$

Model 1 includes AMPA and $GABA_A$ synaptic conductances, and an electrical synapse modeled with NEURON's built-in I_{clamp} point process. Model 2 includes AMPA and NMDA synaptic conductances, along with an electrical synapse modeled with NEURON's built-in I_{clamp} point process. Both models use leakage currents (D'Angelo et al., 2001) and voltage-dependent Na^+, Ca^{2+}, and K^+ conductances (D'Angelo et al., 2001; see Table 1).

All ion conductances were previously shown to be present in mature rat cerebellar granule cells (D'Angelo et al., 1997). These currents (Table 1) are used in the absence of experimentally characterized ion conductances in granular cells of mormyrid ELL, with the assumption of homology between these two groups of granule-type cells. Gating kinetics, taken from D'Angelo et al. (2001), were previously adjusted to account for differences between experimental temperature (D'Angelo et al., 2001) and simulated temperature (T_{sim}=30°C).

Leakage Currents

The presence of $GABA_A$ receptors on mormyrid ELL granular cells (Han et al., 2000) provided a rationale for including a $GABA_A$ dependent Cl^- leak current, especially considering the large LMI calyx surrounding the granular cell soma (Han et al., 2000). Slow ionic currents mediated by a $GABA_A$ dependent Cl^- leak, along with a nonspecific mixed-affinity ion channel leak previously identified in rat cerebellar granule cells (D'Angelo et al., 2001), are included in all models. The nonspecific leakage is set at a current density of 5.68 X 10^{-5} S/cm^2, with a reversal potential of –59mV. The $GABA_A$ mediated leak is set at a current density of 2.17 X 10^{-5} S/cm^2, with a reversal potential of –65mV.

Na^+ currents (I-NaF, I-NaP, I-NaR)

Although the three subpopulations of Na^+ conductances included in the models are similar in their voltage dependence (activating with depolarization) and sensitivity to tetrodotoxin (TTX), each exerts a distinct influence on the behavior of membrane voltage. The fast (I-NaF) and persistent (I-NaP) Na^+ conductances were previously identified in mature rat cerebellar granule cells (D'Angelo et al., 1998). The resurgent (I-NaR) conductance, also taken from D'Angelo et al. (2001), supports repetitive firing by virtue of its rapid transition from open to closed states via a blocked state following repolarization (bypassing inactivation). I-NaR is likely carried by a subpopulation of NaF channels containing the NaV1.6 □ subunit (Raman and Bean, 2001), which is thought to mediate the above-mentioned properties of the channel.

The fast Na^+ current, I-NaF, is responsible for the depolarizing phase of the classical Hodgkin-Huxley (1952) action potential. Although the fast Na^+ channel is effective at providing brief, large depolarizing currents in the spiking neuron, it cannot account for many of the complex current-voltage responses of neurons such as fast repetitive firing, bursting, and subthreshold resonance (D'Angelo et al., 2001). These more sophisticated electrical responses require the involvement of I-NaP and I-NaR.

The persistent sodium channel, which carries I-NaP, activates more slowly than NaF and at a more hyperpolarized membrane potential. NaP also does not inactivate, which allows it to remain open for an extended period of time after initial depolarization. I-NaP has been shown to amplify ionotropic glutamatergic EPSPs below the threshold for spike generation (Berman, Dunn, and Maler, 2001), and to act in concert with the slow, muscarinic K^+ current, I-KM, to control the duration of bursting events during which spikes are rapidly generated from a plateau depolarization (D'Angelo et al., 2001).

Ca^{2+} Membrane Current (I-CaHVA) Intracellular Dynamics

A single species of voltage-gated calcium channel, the N-type high voltage-activated neuronal subtype (CaHVA), is used in all models to tune spike width, attenuation, and threshold sensitivity (via interactions with I-KCa). The current mediated by this channel was previously described in rat cerebellar granule cells in situ by Rossi et al. (1994). Modeling of intracellular Ca^{2+} dynamics, taken from D'Angelo et al. (2001), was necessary for computation of I-CaHVA inactivation and I-KCa gating. The following equation is used to determine intracellular Ca^{2+} concentration:

$$d[Ca^{2+}]/dt = -I_{ca}/(2F\ Ad) - (\beta_{Ca}([Ca^{2+}] - [Ca^{2+}]_o)) \quad (7)$$

where F is Faraday's constant (9.649×10^4 coulombs per mole), d is the depth of the shell adjacent to the internal membrane surface of area A, β_{Ca} is a constant describing the rate of Ca^{2+} buffering via various intracellular fluxes, diffusion, and Ca^{2+} proteins, and $[Ca^{2+}]_o$ indicates extracellular Ca^{+} concentration at rest. As in D'Angelo et al. (2001), Ca^{2+} dynamics are set to produce Ca^{2+} transients on the order of 1μM. Ca0 is taken from measurements of rat cerebellar granule cells in culture (Irving et al., 1992), and the following parameters are used in equation (7) above: d = 200nm, β_{Ca} = 1.5, and $[Ca^{2+}]_o$ = 100nM.

K^{+} Currents (I-KV, I-KM, I-KCa, I-KIR, I-KA)

Five voltage-gated potassium channels previously shown to be expressed in rat cerebellar granule cells (D'Angelo et al., 2001), all conducting outward hyperpolarizing current, are included in the models. Gating kinetics, activation, and inactivation parameters are taken from D'Angelo et al. (2001), and channel densities on the membrane are adjusted to optimally fit target ELL granular cell voltage outputs as a function of input synaptic conductances.

The first group of potassium channels, I-KV, I-KA, and I-KCa, contributes to the hyperpolarizing downstroke of the action potential spike. I-KV is a typical delayed rectifier, Hodgkin-Huxley (1952) type channel that provides hyperpolarizing current to counteract I-NaF during the spike. I-KV activates rapidly following strong depolarization, and does not inactivate but rather exhibits a rapid exponential decay with time after opening. I-KA, the afterhyperpolarizing current, is also fast activating but differs from I-KV in that it inactivates as a function of voltage and tends to exert its hyperpolarizing effects slightly later in the action potential downstroke. I-KA is also more prominent near spike threshold than is I-KV. I-KCa exhibits dual activation dependence on depolarizing voltage and intracellular Ca^{2+} concentration. The functional significance of I-KCa during a bursting event is progressive spike attenuation due to Ca^{2+} accumulation.

The second group of K^{+} channels, I-KIR and I-KM, tends to be active at subthreshold membrane potentials. I-KIR is an inwardly rectifying channel that activates at membrane potentials close to resting (between –80 and –65mV) and inactivates during a spike or bursting event. The overall effect of I-KIR is to help the membrane potential return to rest following long depolarizing events such as repetitive firing and bursting.

The final K^{+} channel included in the models, I-KM, carries the slow-activating, non-inactivating, muscarinic sensitive, TEA insensitive K^{+} current shown by D'Angelo

et al. (2001) to be necessary for intrinsic bursting and resonance in rat cerebellar granule cells. This current activates with the first depolarizing upstroke and continues to increase slowly during a burst until it eventually prevents spike initiation.

Electrical Synapses

Electrical synaptic currents to the model granular cell are simulated as direct current injections (I_{clamp} point process in NEURON simulator) coincident with the onset of chemical synaptic currents. The duration of the current injection was set at 3ms to match the width of the incoming presynaptic action potential. Because the exact degree of attenuation between these cells is unknown, the current amplitude was allowed to vary in accordance with experimentally defined limitations on the relative sizes of the juxtalobar and primary afferent PSPs, as well as with the experimentally suggested voltage outputs of the granular cell itself.

Glutamatergic Synapses and EPSPs

Glutamatergic EPSP shapes are implemented both from an eariler model of turtle cerebellar granule cell □-amino-3-hydroxy-5-methyl-4-isoxazolepropionic acid (AMPA) and N-methyl-D-aspartate (NMDA) synapses (Gabbiani, Midtgaard, and Knopfeel, 1994), and as artificial synapse functions contained in the NEURON simulation package. In both cases, free parameters include maximal inward depolarizing conductance (g_{bar}), rise time constant (τ_{rise}), and decay time constant (τ_{decay}). The reversal potential for these conductances was set to 0mV (Gabbiani et al., 1994). The following equation describes the Na^+ conductance of both AMPA and NMDA receptors used in models 1 and 2:

$$gGlutR(t) = g_{bar}(GlutR)\ (\exp(-t/\tau_{decay})-\exp(-t/\tau_{rise})) \quad (8)$$

where g_{bar} is the maximum conductance associated with the receptor, and the following two terms describe the time course of this conductance. Values for τ_{rise} and τ_{decay} were initially set at experimentally reported levels, reported in Gabbiani et al. (1994), of 0.09ms:1.5ms (AMPA) and 3ms:40ms (NMDA). EPSPs driven by juxtalobar input to ELL granular cells, as measured intracellularly in primary afferents by Bell (1989), are fit well using a τ_{rise} negligibly above 0ms and a τ_{decay} of around 3ms. The gap junction between ELL granular cells and their innervating primary afferent may act as a high-pass filter (Bell, unpublished). This suggests that the EPSP, as it appears in the ELL granular cell, has components with longer τ_{decay} constants and possibly larger amplitudes than are evident from these primary afferent recordings.

GABAergic Synapses ($GABA_A$) and IPSPs

GABAergic LMIs are excited by extracellular K^+ accumulation following granular cell depolarization (Han et al., 2000). Although this mechanism is not explicitly modeled here, the effects of LMI activation are retained by delivering a $GABA_A$ mediated IPSPs to the model granular cell. When included, the timing of these IPSPs is determined by the constraint of burst offset at experimentally suggested post-EOCD latency. IPSPs are modeled similarly to the AMPA-mediated EPSPs described above, with τ_{decay} times ranging between 3 and 15ms (Gabbiani et al., 1994) and a reversal potential of –65mV (set to resting potential for sake of simplicity).

Table 1. Voltage-dependent conductance parameters (from D'Angelo et al., 2001)

Conductance state variables	n	V_{rev} (mV)	α(sec^{-1})	β(sec^{-1})
gNaF				
Activation	3		0.9(V+19)/(1-exp(-(V+19)/10))	36exp(-0.055(V+44))
Inactivation	1	87.39	0.315exp(-0.3(V+44))	4.5(1+exp(-(V+11)/5))
gNaR				
Activation	1		0.00024-0.015(V-4.5)/((exp(-(V-4.5)/6.8)-1))	0.14+0.0.047(V+44)/exp((V+44)/0.11)-1))
Inactivation	1	87.39	0.96*exp(-(V+80)/62.5)	0.03*exp((V+83.3)/16.1)
gNaP				
Activation	1	87.39	0.091(V+42)/(1-exp(-(V+42)/5)) x=1/(1+exp(-(V+42)/5)) τ=5/(α+β)	0.062(V+42)/(1-exp((V+42)/5))
gKV				
Activation	4	-84.69	0.13(V+25)/(1-exp(-(V+25)/10))	1.69exp(-0.0125(V+35))
gKA				
Activation	3		14.67/(1+exp(-(V+9.17)23.32))	2.98(exp(-(V+18.28)/19.47))
Inactivation	1	-84.69	0.33/(1+exp((V+111.33)/12.84)) x=1/(1+exp(-(V+46.7)/19.8)) y=1/(1+exp((V+78.8)/8.4))	0.31/(1+exp(-(V+49.95)/8.9))
gKIR				
Activation	1	-84.69	0.4exp(-0.041(V+83.94))	0.51exp(0.028(V+83.94))
gKCa				
Activation	1	-84.69	2.5/(1+(1.5e-3*exp(-0.085V)/[Ca]))	1.5/(1+[Ca]/(0.15 *10^{-3} *(-0.085V)))
gCaHVA				
Activation	2	129.33	0.15exp(0.063(V+29.06))	0.24exp(-0.039(V+18.66))
Inactivation	1	*	0.0039exp(-0.055(V+48))	0.0039exp(0.012(V+48))
gKslow				
Activation	1	-84.69	0.008exp(0.025(V+30)) x=1/(1+exp(-(V+30)/6))	0.008exp(-0.05(V+30))

This table reports the equations used to calculate τ_x, α_x, τ_y, α_y (see Eqs. 3 and 4) for the membrane conductances used in the model. The number of gating particles (n) and ionic reversal potential (* resting value for Ca^{2+}) used to calculate ionic currents are also shown.

Results

Granular cells receiving projections from mormyromast receptors were modeled as a single compartment soma containing nine intrinsic membrane currents, as shown in Table 1. Synaptic inputs to the granular cell included AMPA- and NMDA-type depolarizing currents from primary afferent and juxtalobar fibers, a depolarizing step current from the primary afferent fiber (electrical synapse), and a $GABA_A$-type shunting current delivered by an LMI cell. Properties of the models were explored by recording voltage responses at the soma as synaptic inputs and intrinsic membrane currents were modified within the range of experimentally defined constraints.

These constraints included the requirement of both electrical and glutamatergic inputs from the primary afferent onto the granular cell, glutamatergic input from the juxtalobar fiber (EOCD) onto the granular cell, a lower limit on the decay time and amplitude of the EPSP produced by the EOCD juxtalobar input to the granular cell (fig. 2), and dependence of spike number output on the relative timing of primary afferent and juxtalobar inputs (fig. 3). Other elements of the model were varied to produce results consistent with the hypothesized coding transformation of latency into spike number (fig. 4).

The physiological dynamic range of post-stimulus firing latencies in the mormyromast primary afferent fiber is around 6ms, where a latency of 0ms would produce a granular cell input directly coincident with the arrival of the juxtalobar EOCD (fig. 3, Bell and Grant, 1992). Six spikes were generated in the granular cell following coincident arrival of the juxtalobar EOCD and primary afferent inputs (fig. 4, Bell and Grant, 1992). Although these field recordings are not representative of the complete range of responses for all granular cells of mormyromast ELL (some cells showed responses following the arrival of primary afferent impulses up to 30ms post-EOCD), the maximum offset latency (~50ms) and spike number of the granular cell response under these conditions (Bell and Grant, 1992) were used as initial constraints on the model.

Following initial testing of a single compartment model that used maximum ionic conductances from the D'Angelo et al (2001) model of rat cerebellar granule cells (see *Preliminary Model)*, two models were created. Model 1 (Table 2; figs. 5, 8) was created

	Preliminary Model	Model 1	Model 2
Primary afferent inputs	None	AMPA, electrical	AMPA, NMDA, electrical
Corollary discharge inputs	None	AMPA	AMPA, NMDA
Large multipolar interneuron inputs	None	$GABA_A$	None
Long depolarizing step current ?	Yes	No	No

Table 2: Summary of models in the present study. See Table 1 for full description of ionic currents.

to maximize the fit to the spike number transformation for a single compartment granular cell. This model, despite closely approximating experimental results, requires use of input characteristics that have yet to be identified *in vivo*. Model 2 (Table 2; figs. 5, 8) was built to retain the fit to coding constraints while gradually eliminating speculative input characteristics. In model 2, the desired relationship between spike number and input delay is achieved only by allowing the total granular cell response to extend over a time window of approximately 100ms greater duration than has been observed *in vivo*.

The input PSPs and maximum ionic conductances of both models were systematically varied to explore the parameter space suggested by experimental data. In addition, total voltage and current responses of simulated granular cells are shown to provide an integrative understanding of the mechanism of latency to spike number transformation.

Preliminary Model

A single compartment granular cell model was created with *default* ionic conductances taken from the D'Angelo et al (2001) model of rat cerebellar granular cell bursting and resonance. As a test of this preliminary model, a constant depolarizing current of 5.7pA was applied to the cell for 300ms. Ionic conductances were varied in an attempt to modulate spike frequency and spike number within the resulting burst. With default conductance levels, a burst lasting 80ms and containing 5 spikes is produced (fig. 6). Onset and offset of the burst are controlled by the balance between the slow, noninactivating Na^+ and K^+ conductances, I-NaP and I-KM (fig. 6, 7b, 7c). Spike attenuation and recovery during the burst are modulated by the I-KCa and I-CaHVA system, as shown in current traces (fig. 7a).

It was not possible to produce a burst of variable spike number (see fig. 6 for experimental records) that depends on the latency between two AMPA/NMDA mediated EPSPs and an I_{clamp} simulating the primary afferent electrical synapse with these default conductance levels. This was due to a lack of regenerative spiking. Realistic cellular inputs such as these produce a two spike output of variable onset latency, regardless of the delay between inputs (not shown). Ionic conductances and synaptic inputs were modified in subsequent models due to the failure of the preliminary model to replicate the experimentally defined relationship between input delay and granular cell spike number (fig. 4): model 1 was created to test the feasibility of the spike number coding hypothesis under conditions of intrinsically controlled burst offset. Model 2 was created to test the necessity of this additional input (LMI controlled GABAergic inhibition).

I-NaP and I-KM sensitivity

As reported by D'Angelo et al. (2001), the bursting response of this model cell under constant current injection is exquisitely sensitive to a balance between the slow, noninactivating I-NaP and I-KM conductances. The burst is eliminated by either a 7.5% decrease in I-NaP maximum conductance or a 5% increase in I-KM maximum conductance (fig. 7b and 7c, respectively).

Modifying these maximum conductances in their respective opposite directions has the efftect of decreasing latency to burst onset and decreasing burst length and spike number. This attenuation is due to saturating depolarization in both cases, i.e. gradual inactivation of I-NaF channels following each of the first several spikes in the burst.

Model 1: Compound EPSPs, IPSP-controlled burst offset

The maximum conductance values of each channel type and the decay time of respective EOCD and primary afferent EPSP inputs to the granular cell were varied in order to more closely fit the voltage behavior of the model to experimental data. A GABAergic IPSP (τ_{decay}=15ms, reversal potential= -65mV, maximum conductance = 5nS) was delivered to the granular cell at 57ms post-EOCD onset in order to limit the length of the burst to experimentally shown response duration in these cells. Although such a burst-ending role has not been shown for LMI cells *in vivo*, it is possible that accumulation of extracellular K^+ in the cleft between the granular cell soma and the presynaptic LMI terminal during the burst could trigger GABA release via ephaptic depolarization (Han et al., 2000). A mechanism whereby GABA release was inhibited during the early part of the burst, via presently uncharacterized connections between the juxtalobar or afferent fibers and the LMI cell, would enable this IPSP to be relatively time-locked to the onset of EOCD or primary afferent inputs to the granular cell.

Although chemically mediated EPSPs delivered onto the granular cell have yet to be described intracellularly, intracellular recordings from the innervating primary afferent suggest that the major component of these EPSPs is more similar to a fast AMPA-like PSP than to a slow, NMDA-like PSP (fig. 5, Bell and Grant, 1992). For this reason, the inputs of model 1 included a primary afferent AMPA and electrical synapse (I_{clamp}), an EOCD AMPA synapse, and the LMI generated IPSP (fig. 8a). The primary afferent AMPA conductance had a reversal potential of 0mV, a maximum conductance of 250pS, and a τ_{decay} of 3ms. The EOCD AMPA synapse was nearly identical, with a reversal potential of 0mV, maximum conductance of 255pS, and a τ_{decay} of 3ms. The amplitude of the primary afferent-delivered I_{clamp} current is 5.77pA, with 3ms duration. Voltage outputs of the model show the desired negative trend in granular cell spike number as a function of increasing synaptic input delays (figs. 4, 9).

Model 1, Overall Ionic Conductance Sensitivities

To test the biological plausibility of the ionic conductance levels and synaptic inputs provided by model 1, four-level sensitivity tests were performed on each conductance type. Maximum conductance for each type was set at 50, 90, 110, and 150% of the model value, holding all other maximum conductances fixed. Spike number was then plotted as a function of delay between inputs (fig. 10).

It was possible to separate conductances into groups having different effects on this relationship within this range of variation. For instance, varying the three conductances of I-NaR, I-KA, and I-CaHVA had the effect of tuning the spike number vs. delay relationship within a range that could still conceivably support the desired neural code (fig. 10). On the other hand, variation of the I-KIR, I-NaF, and I-KV conductances within this range produced situations in which the slope of spike number as a function of delay reached zero (fig. 10). It should be noted that, as expected, increasing the maximum values for depolarizing currents tended to flatten the response at non-zero spike numbers due to I-NaF saturation, while increasing the maximum values for hyperpolarizing currents tended to flatten the response at a spike number of zero.

Additional sensitivity tests were performed on the model to determine the dependence of the spike number vs. delay relationship on maximum AMPA input

conductances, as well as on the complete set of intrinsic ionic conductances described previously. The number of spikes produced in the granular cell as a function of input delay maintained a decreasing trend at maximum AMPA conductances between 50% and 105% of the set value for model 1. A constant number of spikes at all delays were seen for maximum AMPA conductances of 150% and above.

Model 1, I-NaP and I-KM sensitivities

To examine the sensitivity of the model to the balance between I-NaP and I-KM, an extensive parameter space search was performed (holding all parameters fixed except I-NaP and I-KM). Contour plots of spike number as a function of the maximum conductances for these two currents at varying input delays reveal a response topology of relatively invariant shape that translates toward areas of increased maximum I-NaP conductance and decreased maximum I-KM conductance as the delay goes from 0 to 6ms (fig. 11).

It is apparent from these figures that the temporal sensitivity of the spike number response to delay time results (in part) from the model's location (I-NaP=100%, I-KM=100%) on a steep gradient on the parameter contour surface. This gradient extends bidirectionally toward areas of either increased I-NaP and I-KM maximum conductances or decreased I-NaP and I-KM maximum conductances, while most other areas on the contour surface lack a sufficient, properly directed gradient to support the desired relationship between spike number and delay. The model was quite sensitive to small independent changes in either of these two conductances, although its desired response remained robust while the ratio between the two conductances was held relatively constant.

Model 2: Compound EPSPs, intrinsically controlled burst offset

Although model 1 closely approximated the granular cell's coding constraints (production of bursts containing varying numbers of spikes as a function of input delay; see fig. 4), the use of an arbitrarily controlled, LMI delivered IPSP to maintain constant post-EOCD burst offset times was included only to maximize the fit to experimental granular cell responses and the theoretical burst duration code. The precise role of inhibition from the LMI cell onto the granular cell soma at the level of single afferent excitation is unknown *in vivo*, and therefore model 2 was created to maintain the desired granular cell response properties with an intrinsically controlled burst offset.

Model 2, Inputs

The single compartment granular cell in model 2 was given an EOCD AMPA synaptic current with reversal potential of 0mV, τ_{decay} of 2.7ms, and maximum conductance of 270pS (fig. 12). An NMDA component of the EOCD glutamatergic input to the granular cell, with reversal potential of 0mV, τ_{decay} of 40ms, and maximum conductance of 60pS, was included to provide baseline depolarization at the longer time window of bursting exhibited in this model (fig. 12). The chemical components of the primary afferent input for this model were identical to those of the EOCD input except for a slightly lower maximum AMPA conductance in the primary afferent input (250pS). The primary afferent also delivered an electrical synaptic input with a 3ms duration and amplitude of 4pA (fig. 12).

Model 2, Maximum Ionic Conductances

A 50% increase in the maximum I-KCa conductance and a 30% decrease in the maximum I-NaP conductance are the only significant differences in ionic conductances between model 2 and its extrinsically controlled counterpart, model 1 (figure 5). This increased hyperpolarizing conductance and decreased depolarizing conductance in model 2 allows the slow K^+ conductance (I-KM) to overtake the noninactivating depolarizing effects of I-NaP and to eventually end the burst without the influence of synaptic hyperpolarizing currents. In this fashion, the number of spikes produced by the granular cell as a function of delay is controlled by the translation of differing initial summated levels of depolarization into a range of latencies to the initial spike in the burst. Burst onset latency ultimately sets the number of spikes in the response, because larger latencies correspond to higher I-KM conductance levels at burst onset.

Model 2, Overall Ionic Conductance Sensitivities

Four-level sensitivity tests for model 2 reveal relative dependencies of the spike number response on each ionic conductance that are similar to those seen for model 1, with the exception of I-KCa (fig. 14). Varying the maximum conductance of I-KCa +/- 50% with respect to the value used in model 2 nearly completely flattens the spike number response, in stark contrast to the graded tuning sensitivity of the spike response to this range of I-KCa variation in model 1 (fig. 10). This is consistent with the classification of I-CaHVA as a tuning conductance for model 1, because I-CaHVA and I-KCa act together in a synergistic manner during the action potential upstroke and hyperpolarizing step.

Furthermore, such a finding suggests that intrinsically controlled bursting in the granular cell is controlled by I-NaP / I-KM and I-CaHVA / I-KCa conductance ratios rather than the I-NaP / I-KM ratio alone. This hypothesis could be tested directly *in vitro* by patch clamping of the granular cell soma and application of chemical antagonists specific for each type of ion channel.

Model 2, I-NaP and I-KM Sensitivities

Examination of the spike number contour surface, defined by variations in maximum I-NaP and I-KM conductances over different input delays, reveals a dependence of the graded spike number response on the ratio between these two conductances that is similar to that seen for model 1 (fig. 15). However, an area of uncontrolled repetitive firing on the I-NaP / I-KM contour surface for model 2 is seen when maximum conductances for both channel types approach zero (fig. 15). This is consistent with the D'Angelo et al (2001) finding that bursting activity in the electrotonically compact granule cell requires the presence of both the slow K^+ and persistent Na^+ conductances.

Model 2, Burst Onset and Offset

Although the trend of spike number as a function of input delay for model 2 roughly matches both experimental results and the hypothesized code for stimulus intensity at the granular cell layer (fig. 4), the burst offset latencies for the model cell

response of between 80 and 120ms post-EOCD input are nearly twice as long as those that have been observed *in vivo* (figure 4, 13). Attempts to shorten these offset latencies by increasing the maximum conductances for I-KM and I-KCa eliminate the sensitivity of burst onset latencies to input delay, as shown in sensitivity curves (fig. 14).

Model 2, Summary

The depolarizing force of slow, NMDA-type conductances in model 2 was able to maintain bursting long enough for I-KM to intrinsically repolarize the cell. Sensitivity tests for model 2 (fig. 14) indicate fairly stringent restrictions on the degree to which maximum ionic conductances and maximum input currents can be varied while maintaining the desired graded spike number response in the granular cell across different input delays.

Because model 2 uses a plausible combination of glutamatergic synaptic currents and eliminates the necessity of uncharacterized LMI burst offset control, it is more parsimonious than model 1 in terms of experimentally given input constraints. However, the necessity of LMI-controlled burst-offset latency (model 1) is shown by the large discrepancy between burst offset latencies for model 2 and experimental results (figs. 4, 13), as well as by the sensitivity of model 2 to relatively small changes in maximum ionic conductances (fig. 14).

Discussion

Modeling results of this study show that the transformation from afferent latency to burst duration in the ELL granular cell layer of *Gnathonemus petersii* can be explained by fast, fixed-latency inhibition and the interaction of persistent Na^+ (I-NaP) and slow, noninactivating K^+ (I-KM) channel conductances. Restriction of burst offset times to experimentally described ranges requires precisely timed inhibition, possibly via LMI inhibition at the level of single afferent fiber stimulation. However, it is conceivable that gating kinetics of modeled ion currents differ from granular cell currents *in vivo*. This could alleviate the need for LMI recruitment by providing intrinsic membrane current control of burst-ending repolarization.

Since the physiological range of delays between arrival of EOCD and afferent inputs to the granular cell is brief (Bell and Grant, 1992), and the granular cell is known to be electrotonically compact, the generation of variable length bursts must depend on amplification of initial differences in summated depolarization. Two candidates for such EPSP amplification are the NMDA receptor and I-NaP. In these models, I-NaP was instrumental as a mechanism for such differential amplification. The voltage-dependent Mg^{2+} block on NMDA-R activation was not tested, because the voltage range of summated EOCD and primary afferent EPSPs (between -50 and -40mV) does not match the range of expected maximum Mg^{2+} block voltage-dependence (-70 to -60mV; D'Angelo et al., 1995).

Intrinsic control of burst offset

Although the model successfully accounts for the increase in post-EOCD latency of the first granular cell spike as the delay between the two inputs increases, the corresponding decrease in burst offset latency shown by Bell and Grant (1992; fig. 3b) is fit poorly by both model 1 (fig. 9), with LMI controlled burst offsets, and model 2, with intrinsically ending bursts (fig. 13). However, each model suggests possible solutions to this discrepancy.

Model 2 shows that the gradual rise of the slow, noninactivating potassium current, I-KM, is necessary for intrinsic burst termination. Examination of contour surfaces describing spike number output of the model with varying levels of the maximum conductances for both I-KM and I-NaP reveals that reducing I-KM to zero results in uncontrolled repetitive firing over a broad range of values for I-NaP. This predicted transition to repetitive firing could be tested *in vitro* under appropriate input conditions by application of Cs^+ and/or Ba^{2+} to chemically block I-KM channels, along with application of bicuculline to block $GABA_A$ mediated inputs caused by ephaptic stimulation of LMI presynaptic terminals.

It is possible that the gating kinetics of the I-KM current in ELL granular cells differ from those reported in D'Angelo et al. (2001) for rat cerebellar granule cells. Model 2 suggests that increasing I-KM activation kinetics over a similar voltage range would accelerate burst offset by overtaking the depolarizing effects of I-NaP mediated inward current.

Activation of I-KM at slightly more hyperpolarized membrane potentials would allow for burst onset latency to more directly control burst offset latency. Longer periods of subthreshold depolarization would then increase the proportion of I-KM channels open at the onset of the burst, decreasing the number of spikes that could be produced before I-

KM blocked regenerative effects of both I-NaP and I-NaR. These properties of I-KM gating kinetics could be determined by patch clamping granular cells *in vitro* in the presence of tetraethylammonium (TEA) and chemical agents that selectively block other K^+ channel subtypes while leaving I-KM current intact. Modeling of patch clamp results would then allow characterization of the exponential functions describing kinetics for I-KM .

Another possible mechanism for intrinsic control of burst offset suggested by the models involves the I-KCa / I-CaHVA system. The effect of this system in the present models is limited to minor spike amplitude adaptation and spike number response tuning. However, intracellular Ca^{2+} accumulation during the burst in areas containing dense clusters of I-KCa channels could allow hyperpolarizing effluxes of K^+ to overcome regenerative Na^+ currents and prevent subsequent spikes. *In vitro* patch clamp examination of Ca^{2+} conductance at subthreshold membrane potentials in ELL granular cells, combined with modeling of complete calcium dynamics (e.g. release from intracellular compartments, possible localization at I-KCa channel clusters, or buffering), would allow testing of this hypothesis.

Extrinsic control of burst offset

Restriction of spike responses in the model granular cell to the post-EOCD time window observed experimentally (Bell and Grant, 1992) requires delivery of an IPSP with fixed post-EOCD latency (fig. 8). Although this requirement clearly suggests LMI involvement at the level of single afferent stimulation, invariant IPSP timing cannot easily be accounted for by known anatomical connections between either primary afferent fibers and granular cells, juxtalobar fibers and granular cells, or LMI cells and granular cells.

While granular cell excitation can directly stimulate GABA release from the large LMI terminals that surround the somata of granular cells via extracellular K^+ accumulation (Meek, Grant, and Bell, 1999), it is unclear how this ephaptic excitation could be controlled independently of spike number in the granular cell. It is possible, however, that control of LMI inputs to the granular cell depends on either K^+ accumulations driven by the collective activation of a population of granular cells, or precisely timed ephaptic stimulation of LMI cells by neighboring granular cells receiving afferent impulses at different times.

It is therefore necessary to develop a quantatative method for modeling extracellular, K^+-dependent ephaptic stimulation of GABA release at the calyx onto the granular cell soma (including changes in release rate following repetitive stimulation), and to establish the role of inhibitory LMI synapses onto granular cell dendrites. It is possible that complex dynamics of either K^+ accumulation at the calyx or vesicular fusion and release at the presynaptic LMI terminal could control variable burst offset in the granular cell.

Coregulation and Response Pooling

The fact that close fitting of models 1 and 2 to experimental data depends heavily on the ratio of I-NaP:I-KM maximum conductances (figs. 12, 15) suggests the existence of cellular mechanisms for co-regulation of these two channel types (see Liu et al., 1998 for possible activity-dependent mechanisms) . For example, a decrease in total I-NaP

conductance due to decreased gene transcription rates, post-transcriptional modification of channel subunits controlling activation kinetics, or alterations in channel trafficking and localization, could be expected to accompany down-regulation of total I-KM conductance.

Testing of such co-regulation could be done by comparing the effects of acute I-NaP/I-KM channel blockade in slice preparations with the effects of either chronic channel blockade *in vitro* or partial over-expression of either channel *in vivo*. While sensitivity to acute channel blockade *in vitro* is expected to greatly attenuate the graded nature of the burst duration code in the granular cell, plausibility of this mechanism under noisy biological conditions predicts gradual recovery of the burst duration code during both chronic channel blockade and partial over-expression regimes.

Postsynaptic pooling of granular cell responses, despite potentially decreasing the spatial resolution of the code for local stimulus intensity at the skin, would increase the robustness of the burst duration code by eliminating independent noise created by the variability of single granular cell responses. The transformation from input delay (i.e. primary afferent latency-to-fire) to spike number in the granular cell models varies in its fidelity as maximum ionic conductances, EPSP amplitudes, and EPSP time constants are shifted over a 50% range from set values. This suggests the existence of a biological mechanism for response pooling at the granular cell layer, which would sharpen the electrical image by averaging out noise caused by slight fluctuations in these parameters.

Future Model Directions

These models emphasize the importance of future experiments testing EPSP shapes, relative ionic conductance levels, LMI interactions during granular cell bursting, and coregulation of ionic conductances over long time periods, for more complete understanding of granular cell layer stimulus representations. Improvements to the models that will contribute to this understanding include the use of full Ca^{2+} handling, ephaptic stimulation of LMI presynaptic terminals, precise synaptic locations, inputs from secondary afferents, effects of dendritic and axonal geometry, and differential ion channel densities at various locations on the surface of the granular cell.

Construction of a layer of granular cells receiving input from a corresponding array of mormyromast receptors is the next step toward understanding these representations on an organismal level. This step requires consideration of factors not included at the single cell level, including lateral inhibition from LMI cells, degree of afferent convergence onto the granular cell layer, response pooling (i.e. convergence postsynaptic to the granular cell layer), and the effects of extracellular ion accumulation on the electrical properties of neighboring cells. This degree of sophistication will only be possible once interactions at the single cell level, especially with respect to LMI interactions, are more fully understood.

References

1. Bell CC (1989). Sensory coding and corollary discharge effects in mormyrid electric fish. Journal of Experimental Biology **146**: 229-53.

2. Bell CC and Grant K (1992). Sensory processing and corollary discharge effects in mormyromast regions of mormyrid electrosensory lobe. II. Cell types and corollary discharge plasticity. Journal of Neurophysiology **68**(3): 859-75.
3. Berman, Dunn and Maler (2001). Function of NMDA receptors and persistent sodium channels in a feedback pathway of the electrosensory system. Journal of Neurophysiology **86**(4):1612-21.
4. Brand A, Behrend O, Marquardt T, McAlpine D, and Grothe B (2002). Precise inhibition is essential for microsecond interaural time difference coding. Nature 417:543-547.
5. Carr and Friedman (1999). Evolution of Time Coding Systems. Neural Computation **11**:1-20.
6. D'Angelo E, De Filippi G, Rossi P, and Taglietti V (1995). Synaptic excitation of individual rat cerebellar granule cells in situ: evidence for the role of NMDA receptors. J Physol (Lond) **484**:397-413.
7. D'Angelo E., Nieus T, Maffei A, Armano S, Rossi P, Taglietti V, Fontana A, and Naldi G (2001). Theta-frequency bursting and resonance in cerebellar granule cells: experimental evidence and modeling of a slow K^+-dependent mechanism. Journal of Neuroscience **21**(3): 759-70.
8. Gabbiani F, Midtgaard J, and Knopfel T (1994). Synaptic integration in a model of cerebellar granule cells. Journal of Neurophysiology **72**(2): 999-1009.
9. Han VZ, Grant K, and Bell CC (2000). Rapid activation of GABAergic interneurons and possible calcium independent GABA release in the mormyrid electrosensory lobe. Journal of Neurophysiology **83**(3): 1592-604.
10. Hines M and Carnevale T (1997). The NEURON simulation environment. Neural Comput. **9**(6):1179-209.
11. Hodgkin and Huxley (1952). A quantatative description of membrane currents and its application to conduction and excitation in nerve. J Physiol (Lond) **117**:500-544.
12. Irving AJ, Collingridge GL, and Schoefield JG (1992). Glutamate and acetylcholine mobilize Ca^{2+} from the same intracellular pool in rat cerebellar granule cells using transduction mechanisms with different Ca^{2+} sensitivities. Cell Calcium **13**:293-301.
13. Liu Z, Golowasch J, Marder E, and Abbott LF (1998). A Model Neuron with Activity-Dependent Conductances Regulated by Multiple Calcium Sensors. J Neurosci **18**(7):2309-2320.
14. Meek, Grant and Bell (1999). Structural Organization of the Mormyrid Electrosensory Lateral Line Lobe. J Exp Bio **202**:1291-1300.
15. Raman and Bean (2001). Inactivation and recovery of sodium currents in cerebellar Purkinje neurons: evidence for two mechanisms. Biophys J. **80**(2):729-37.
16. Rossi P, D'Angelo E, Magistretti J, Toselli M, Taglietti V (1994). Age-dependent expression of high-voltage activated calcium currents during cerebellar granule cell development in situ. Pflugers Arch. **429**(1):107-116.
17. Szabo T and Hagiwara S (1967). A latency-change mechanism involved in sensory coding of electric fish (mormyrids). Physiol. Behav. **2**:331-335.

Figure Captions

Figure 1: Schematic showing electric organ corollary discharge (EOCD) involvement in stimulus intensity coding for mormyromast projection pathway of *Gnathonemus petersii*. The present model addresses transformation of the latency code into a burst code for stimulus intensity at the granular cell layer of the electrosensory lateral line lobe (ELL) (modified from Hall and Bell, 1995)

Figure 2a: Conceptual model of inputs to and outputs from granular cell in the medial (mormyromast) zone of electrosensory lateral line lobe (ELL) cortex in *Gnathonemus petersii*. Primary mormyromast afferents create excitatory electrical and glutamatergic synapses onto the soma of the granular cell. Juxtalobar nucleus (jln) input carrying the electric organ corollary discharge (EOCD) is delivered to the granular cell soma via an excitatory glutamatergic synapse. Inhibitory GABAergic input from the large multipolar interneuron is delivered at the granular cell soma. Granular cell axons project to large ganglion and fusiform cells in the plexiform layer of the ELL.

Figure 2b: EOCD EPSPs in mormyromast afferent fibers. Voltage traces show large EOCD EPSP and EOCD-associated field potential. Sweeps are triggered by the command signal. Command signal shown is 3-spike electromotoneuron volley recorded from the tail. In the uncurarized fish, the EOD occurs 1-2ms after the last positive peak of this command signal. Peak-to-peak amplitudes of the command signals in different fish were between 0.1 and 0.2 mV. Positivity near the tail is indicated in the upward direction for the command signal trace. a: EOCD EPSP. b: EOCD-associated field potential recorded just outside the fiber. Positivity is upward. c: subtraction of field potential from intracellular record. (from Bell, 1990).

Figure 3a: Latency to response of a mormyromast afferent fiber as a function of stimulus intensity. Each dot in the raster display represents a spike in the response to an electrosensory stimulus given at time zero. Positions on the abscissa show the times of the different spikes in a response. Positions on the ordinate show the stimulus intensity in millivolts across the skin, at which responses were evoked. Note the smooth change in latency of the first spike as stimulus intensity is increased (modified from Hall, 1995).

Figure 3b: Effects of changes in post-EOCD delay of primary afferent input arrival on number of spikes produced in ELL granular cell. Command signal is indicated by open arrow (bottom), primary afferent arrival at granular layer indicated by filled arrows. Delays between expected EOCD arrival and primary afferent arrival are shown to the left of each sweep, and delays between command signal and primary afferent arrival are shown to the right of each sweep. Note that small changes in delay have a strong effect on the response, and that the trend of decreasing spike number with increasing delay is nearly symmetric with respect to EOCD arrival (Bell and Grant, 1992).

Figure 4: Spike number in ELL granular cells as a function of delay between EOCD and primary afferent inputs. Note that the curve for experimental data was taken from a cell

not showing responsiveness over the complete dynamic range of the primary afferent latencies.

Figure 5a: Relative maximum ionic conductance (gbar) values shown for all channels included in the models. Values are normalized with respect to preliminary model levels.

Figure 5b: Relative maximum ionic conductance (gbar) values shown for each class of channel (Na^+, K^+, and Ca^{2+}) in the present models. Values are normalized with respect to preliminary model levels.

Figure 6: Voltage trace and complete K^+ current traces for preliminary model with default D'Angelo et al. (2001) maximum conductance values. Constant current was applied to the cell over the entire 300ms time window, producing a burst of five spikes. Inward currents are shown as negative values.

Figure 7a: Voltage traces taken from preliminary model under constant current injection for 300ms. Maximum I-KCa conductance was varied over five levels relative to default D'Angelo et al. (2001) values.

Figure 7b: Voltage traces taken from preliminary model with default maximum ionic conductance levels from D'Angelo et al. (2001). Constant current was applied over the entire 300ms time window. The maximum ionic conductance for I-NaP was varied over five levels relative to default D'Angelo et al. (2001) values.

Figure 7c: Voltage traces taken from preliminary model with default maximum ionic conductances from D'Angelo et al. (2001). Constant depolarizing current was applied for the entire 300ms time window. Maximum conductance for I-KM was varied over four levels relative to default D'Angelo et al. (2001) levels.

Figure 7d: Voltage traces for single compartment preliminary model with default maximum ionic conductances from D'Angelo et al. (2001). Constant depolarizing current was applied at the midpoint of the soma for the entire 300ms time window. Current amplitude was varied over five levels relative to default D'Angelo et al. (2001) values.

Figure 8: Complete set of synaptic currents shown for model 1 single compartment granular cell. All synaptic currents were input at the midpoint of the soma. Electrical and glutamatergic components from the primary afferent were given coincident onsets. Each current trace was done in isolation, and a voltage clamp was applied at -40mV to resolve the LMI delivered IPSP.

Figure 9: Voltage traces shown for model 1 at delays of 0, 3, and 5ms between the full EOCD and primary afferent inputs.

Figure 10: Spike number in model 1 granular cell as a function of the delay between EOCD and primary afferent inputs. Each plot displays results for 4 levels of maximum ionic conductances relative to the default model value.

Figure 11: Spike number in model 1 granular cell as a function of relative maximum ionic conductances for both I-NaP and I-KM. Each plot represents a different delay between EOCD and primary afferent inputs.

Figure 12: Current traces for synaptic inputs to model 2 single compartment granular cell. Electrical and glutamatergic components from the primary afferent were given coincident onsets. Each trace was done in isolation.

Figure 13: Membrane voltage as a function of time for model 2 over a range of delays between EOCD and primary afferent inputs. Burst ends intrinsically.

Figure 14: Spike number in model 2 granular cell as a function of input delay between EOCD and primary afferent inputs. Each plot displays results for 4 levels of maximum ionic conductances relative to the default model value.

Figure 15: Spike number in model 2 granular cell as a function of relative maximum ionic conductances for both I-NaP and I-KM. Each plot represents a different delay between EOCD and primary afferent inputs.

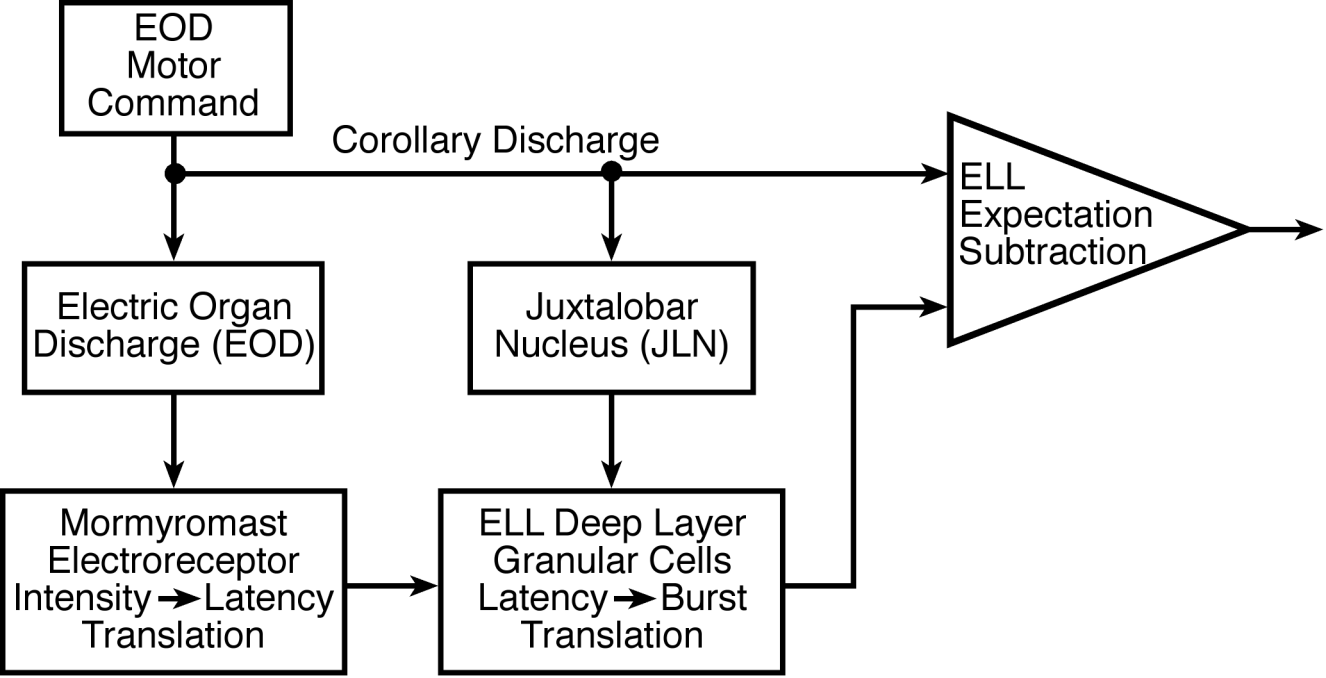
EOD
Motor
Command
Corollary Discharge
ELL
Expectation
Subtraction
Electric Organ
Discharge (EOD)
Juxtalobar
Nucleus (JLN)
Mormyromast
Electroreceptor
Intensity → Latency
Translation
ELL Deep Layer
Granular Cells
Latency → Burst
Translation

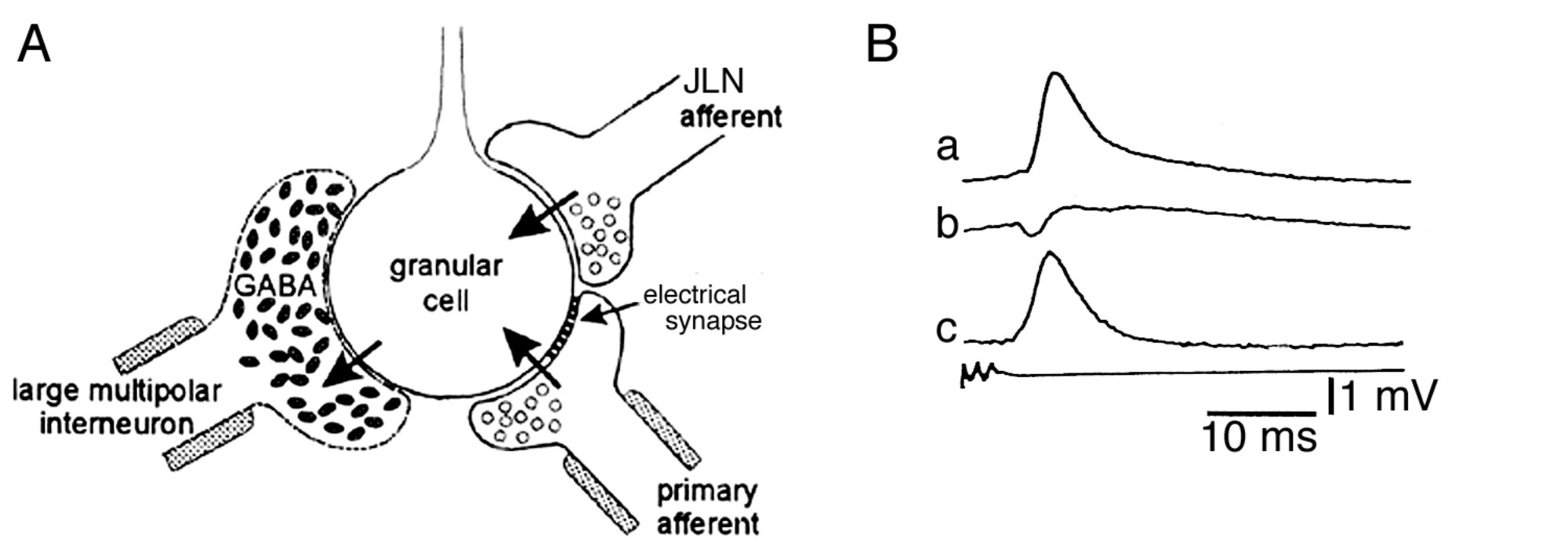
A
JLN
afferent
granular
cell
GABA
electrical
synapse
large multipolar
interneuron
primary
afferent
B
a
b
c
1 mV
10 ms

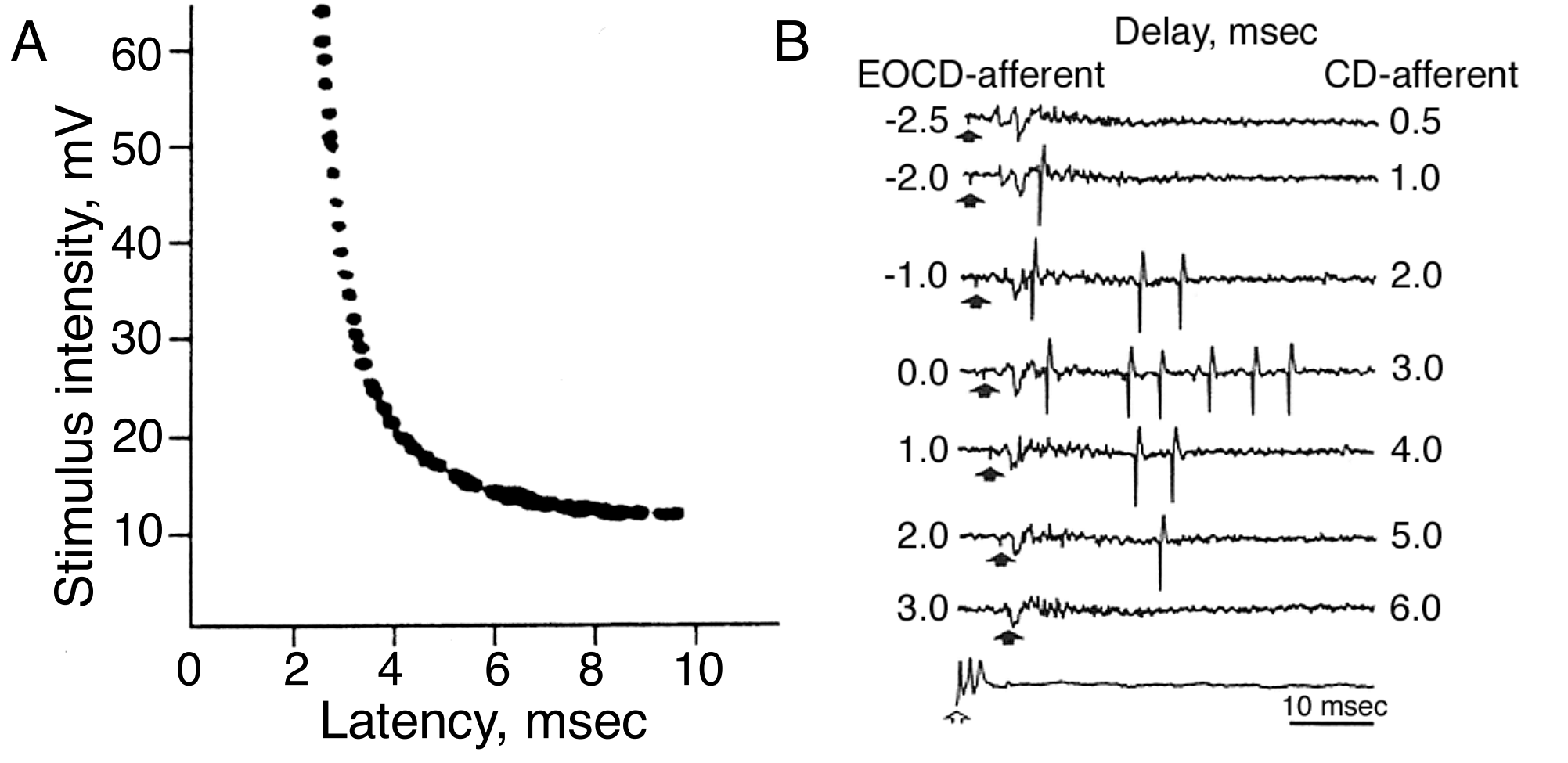
A
Stimulus intensity, mV
60
50
40
30
20
10
0
2
4
6
8
10
Latency, msec
B
Delay, msec
EOCD-afferent
CD-afferent
-2.5
0.5
-2.0
1.0
-1.0
2.0
0.0
3.0
1.0
4.0
2.0
5.0
3.0
6.0
10 msec

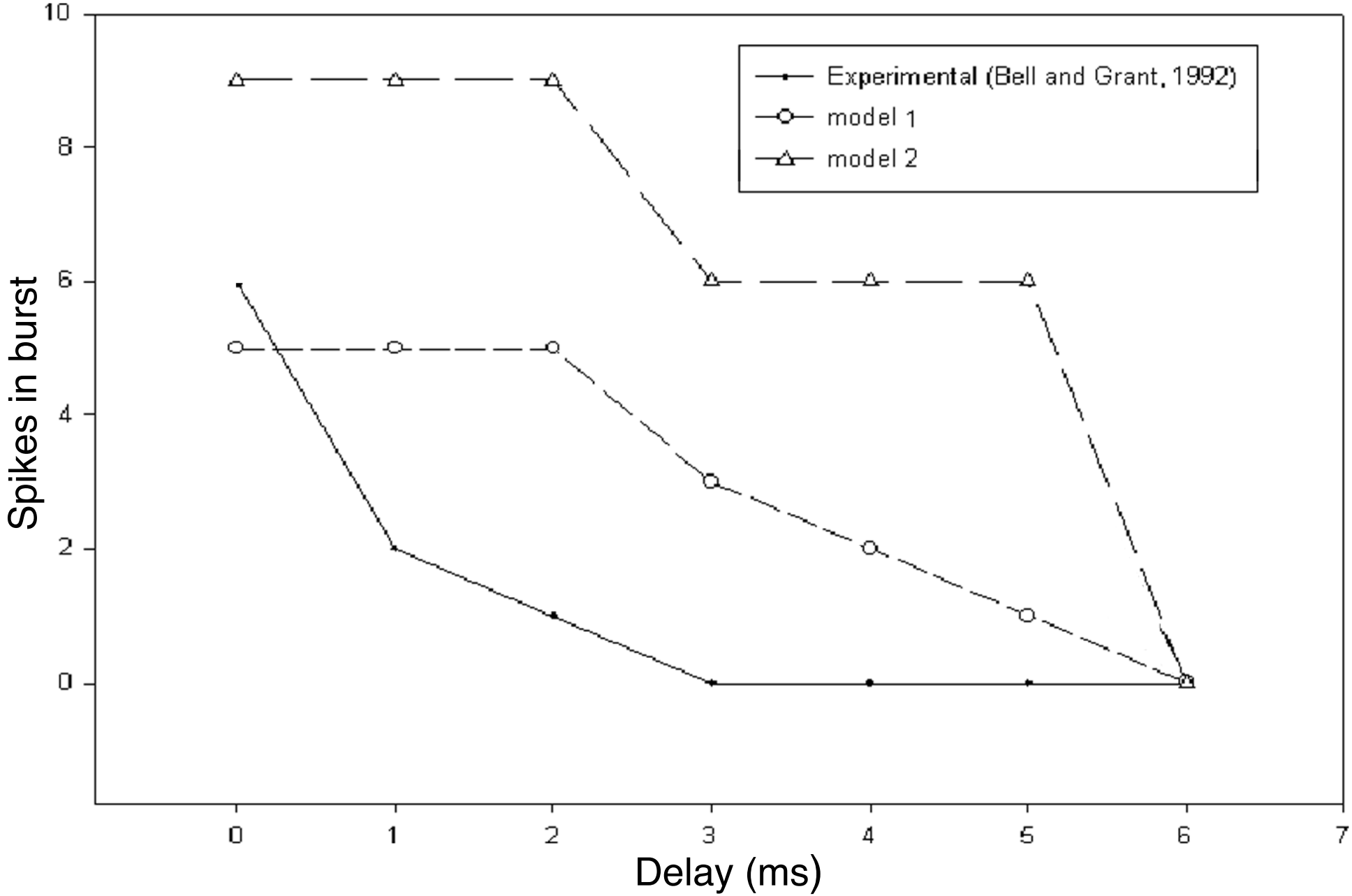
Experimental (Bell and Grant, 1992)
model 1
model 2
Spikes in burst
Delay (ms)
10
8
6
4
2
0
0
1
2
3
4
5
6
7

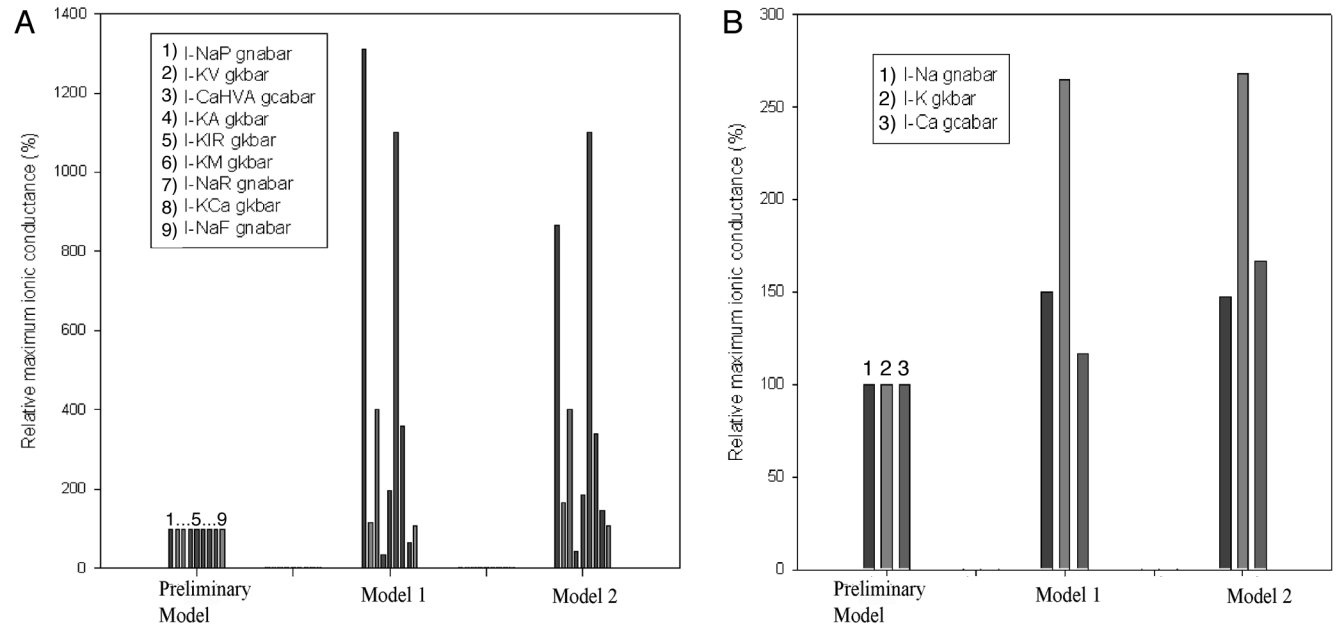
A
1) I-NaP gnabar
2) I-KV gkbar
3) I-CaHVA gcabar
4) I-KA gkbar
5) I-KIR gkbar
6) I-KM gkbar
7) I-NaR gnabar
8) I-KCa gkbar
9) I-NaF gnabar
Relative maximum ionic conductance (%)
1400
1200
1000
800
600
400
200
0
1...5...9
Preliminary Model
Model 1
Model 2
B
1) I-Na gnabar
2) I-K gkbar
3) I-Ca gcabar
Relative maximum ionic conductance (%)
300
250
200
150
100
50
0
1 2 3
Preliminary Model
Model 1
Model 2

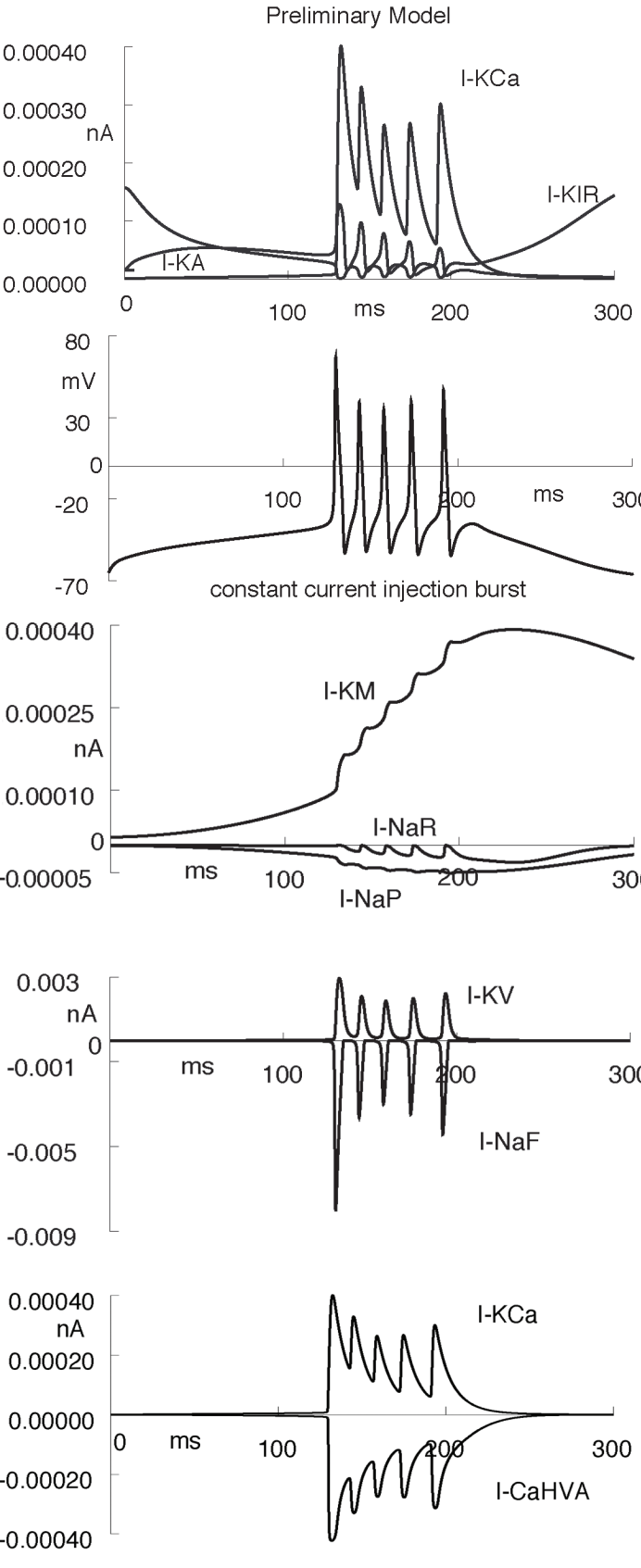
Preliminary Model
0.00040
0.00030
nA
0.00020
0.00010
0.00000
I-KCa
I-KIR
I-KA
0
100
ms
200
300
80
mV
30
0
-20
-70
100
200
ms
300
constant current injection burst
0.00040
0.00025
nA
0.00010
0
-0.00005
I-KM
I-NaR
ms
100
200
300
I-NaP
0.003
nA
0
-0.001
-0.005
-0.009
ms
100
200
300
I-KV
I-NaF
0.00040
nA
0.00020
0.00000
-0.00020
-0.00040
I-KCa
0
ms
100
200
300
I-CaHVA

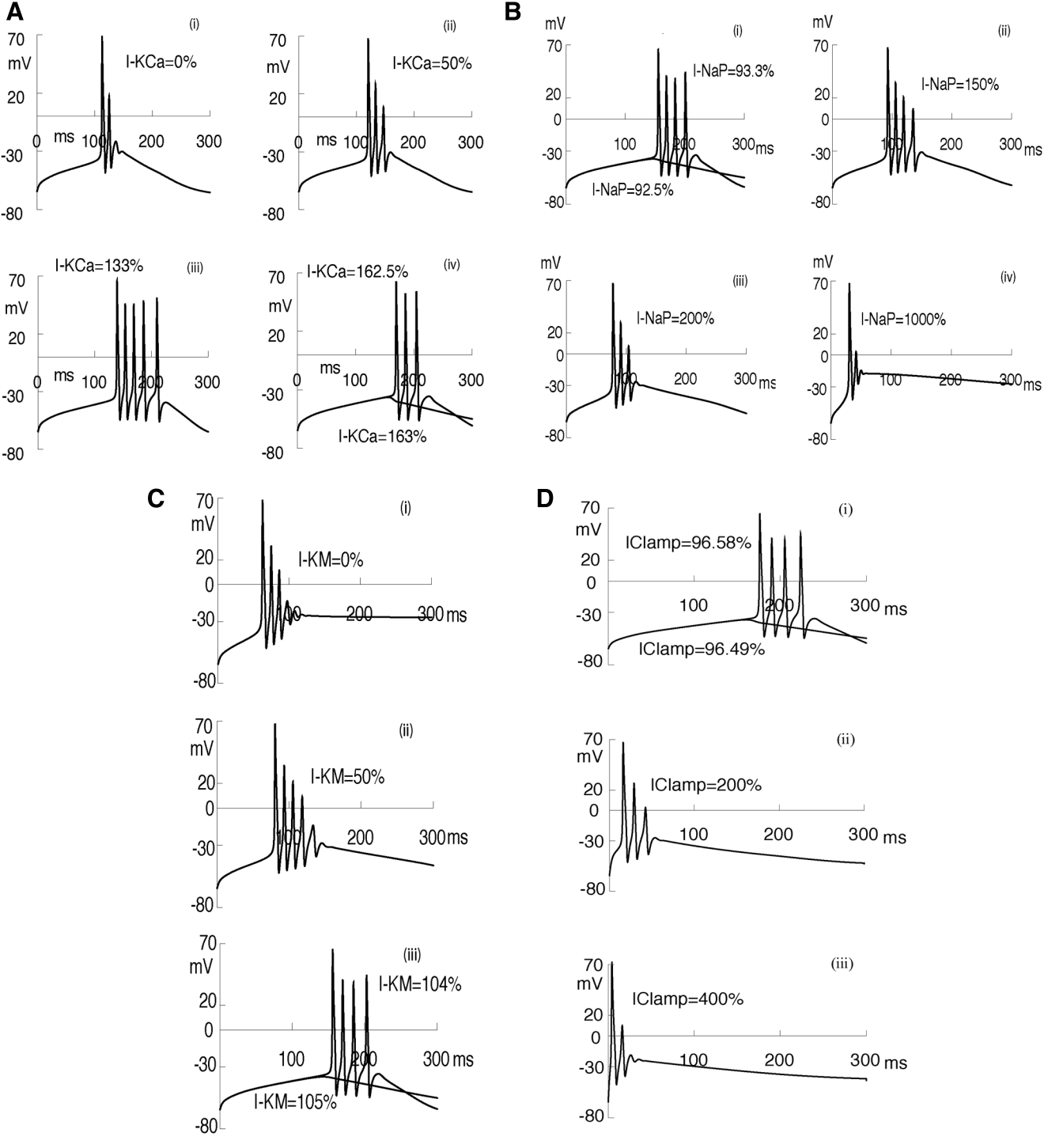
A
(i)
I-KCa=0%
(ii)
I-KCa=50%
(iii)
I-KCa=133%
(iv)
I-KCa=162.5%
I-KCa=163%
B
(i)
I-NaP=93.3%
I-NaP=92.5%
(ii)
I-NaP=150%
(iii)
I-NaP=200%
(iv)
I-NaP=1000%
C
(i)
I-KM=0%
(ii)
I-KM=50%
(iii)
I-KM=104%
I-KM=105%
D
(i)
IClamp=96.58%
IClamp=96.49%
(ii)
IClamp=200%
(iii)
IClamp=400%
mV
ms

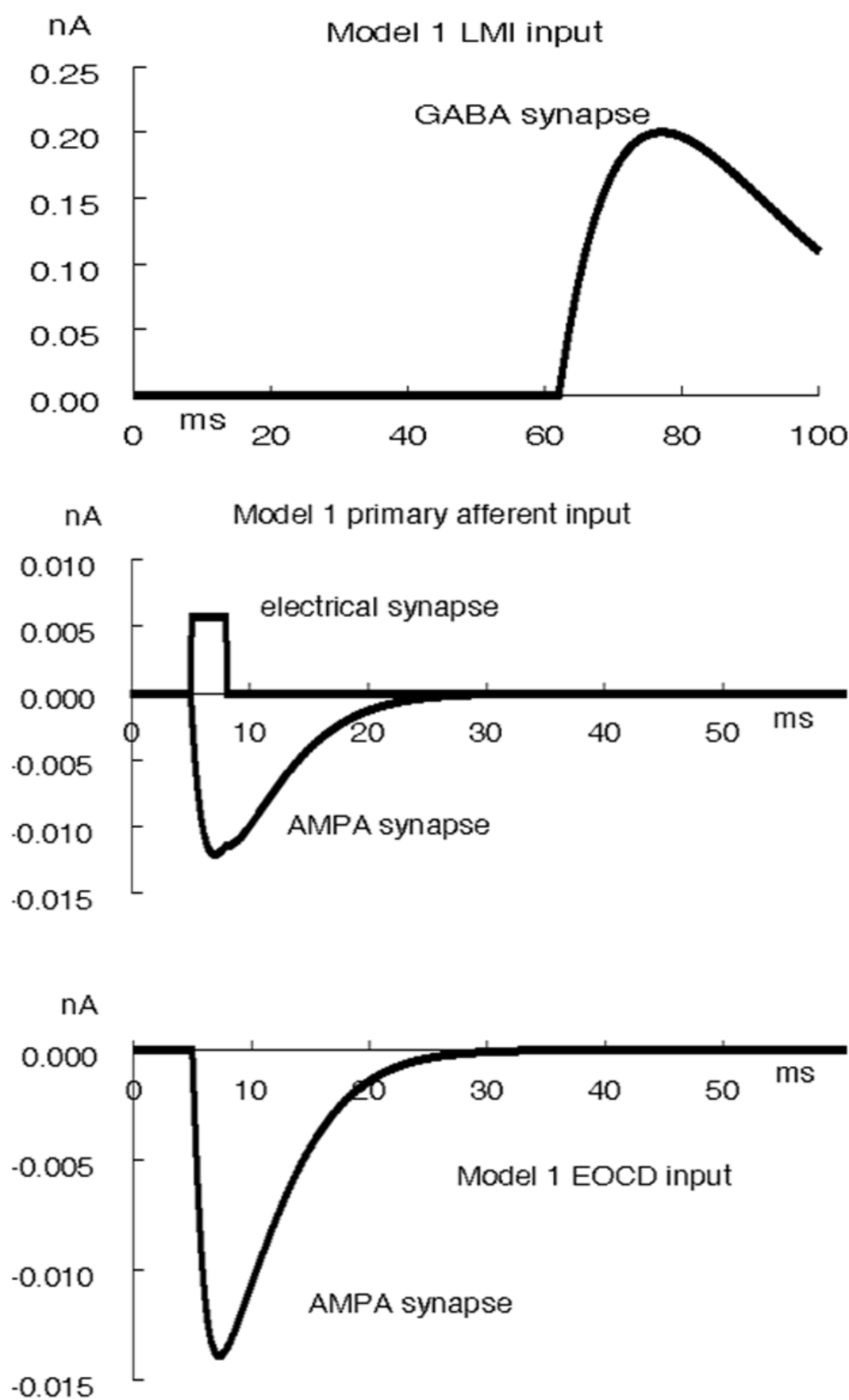
nA
Model 1 LMI input
0.25
0.20
0.15
0.10
0.05
0.00
GABA synapse
0
ms
20
40
60
80
100
nA
Model 1 primary afferent input
0.010
0.005
0.000
-0.005
-0.010
-0.015
electrical synapse
0
10
20
30
40
50
ms
AMPA synapse
nA
0.000
-0.005
-0.010
-0.015
0
10
20
30
40
50
ms
Model 1 EOCD input
AMPA synapse

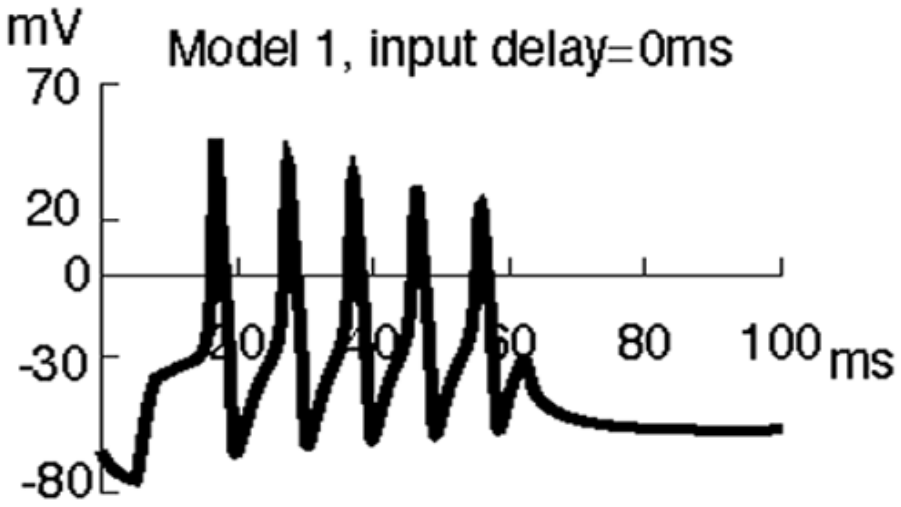
mV
Model 1, input delay=0ms
70
20
0
-30
-80
20
40
60
80
100
ms

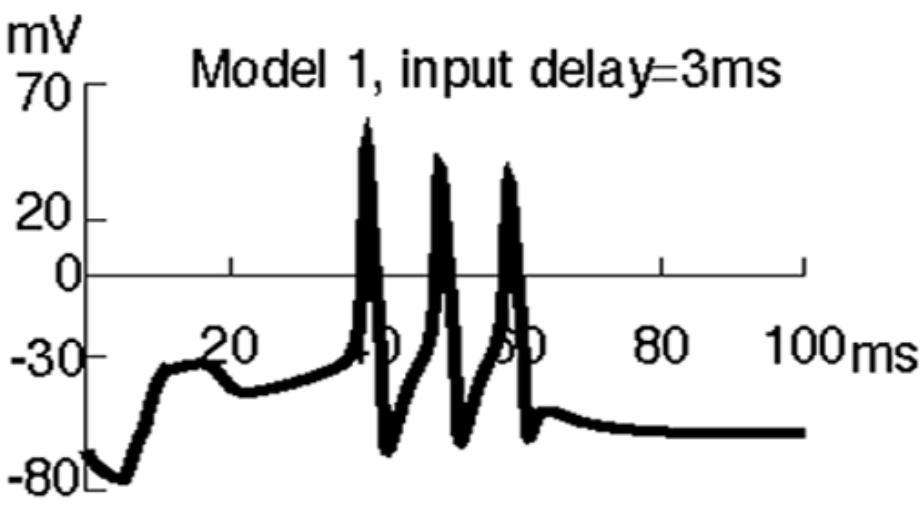
mV
Model 1, input delay=3ms
70
20
0
-30
-80
20
40
60
80
100
ms

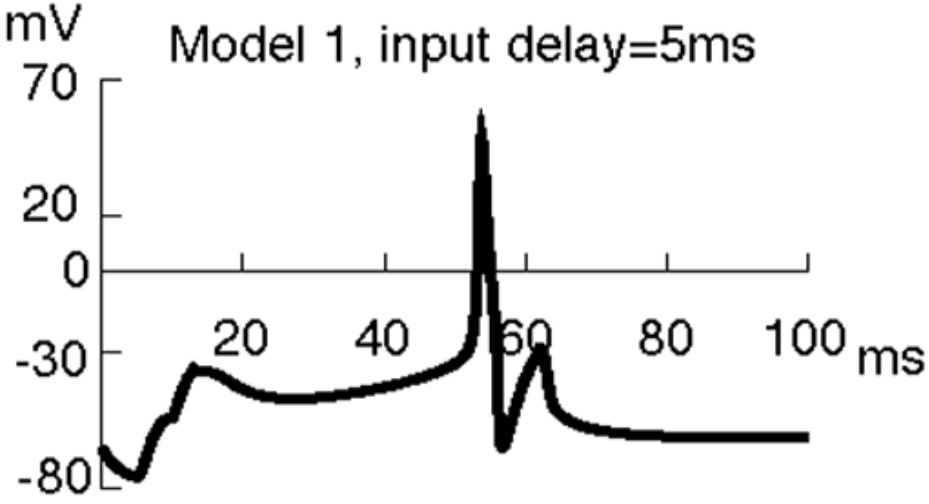
mV
Model 1, input delay=5ms
70
20
0
-30
-80
20
40
60
80
100
ms

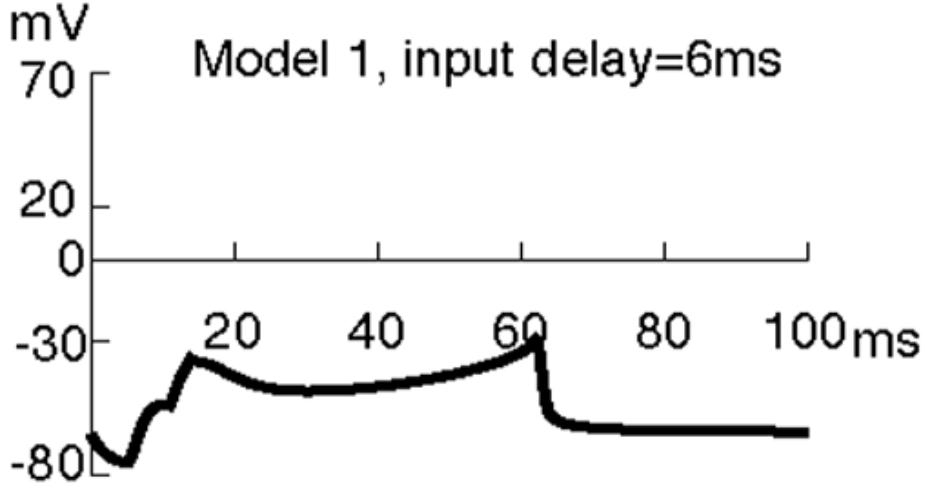
mV
Model 1, input delay=6ms
70
20
0
-30
-80
20
40
60
80
100
ms

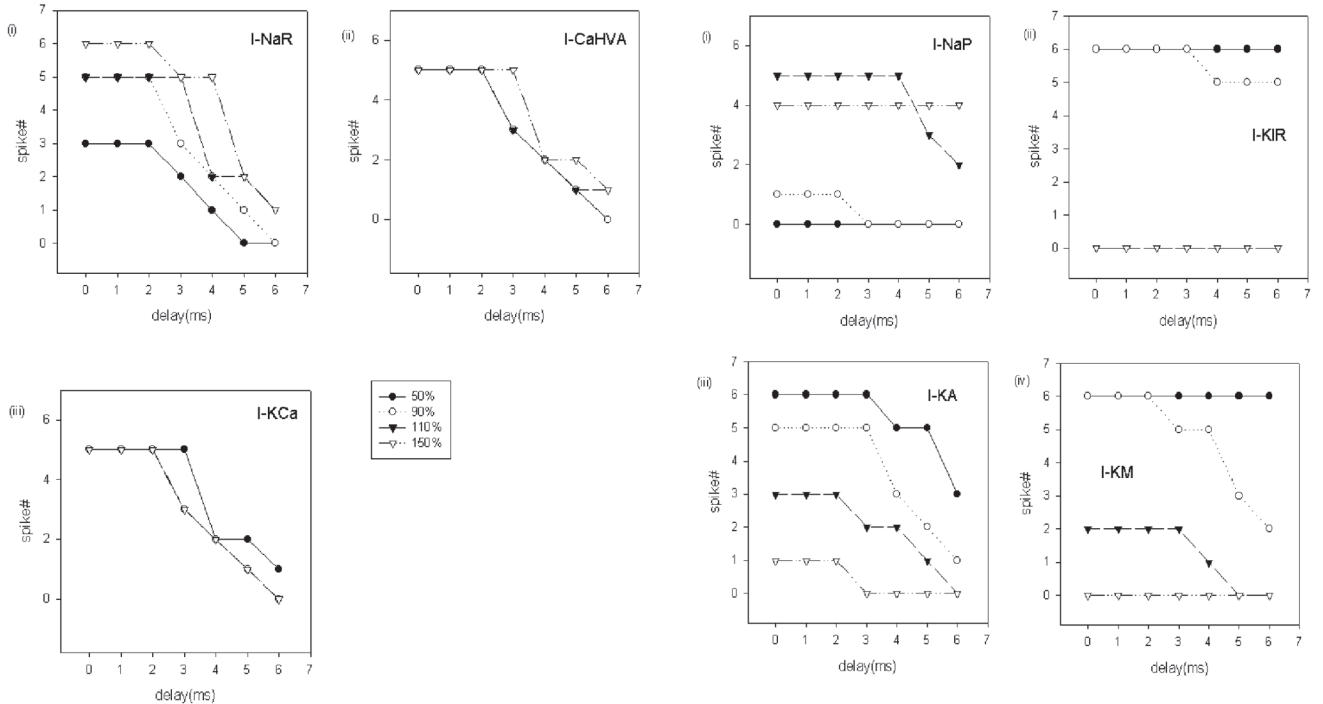
(i)
I-NaR
spike#
delay(ms)
(ii)
I-CaHVA
spike#
delay(ms)
(i)
I-NaP
spike#
delay(ms)
(ii)
I-KIR
spike#
delay(ms)
(iii)
I-KCa
spike#
delay(ms)
50%
90%
110%
150%
(iii)
I-KA
spike#
delay(ms)
(iv)
I-KM
spike#
delay(ms)

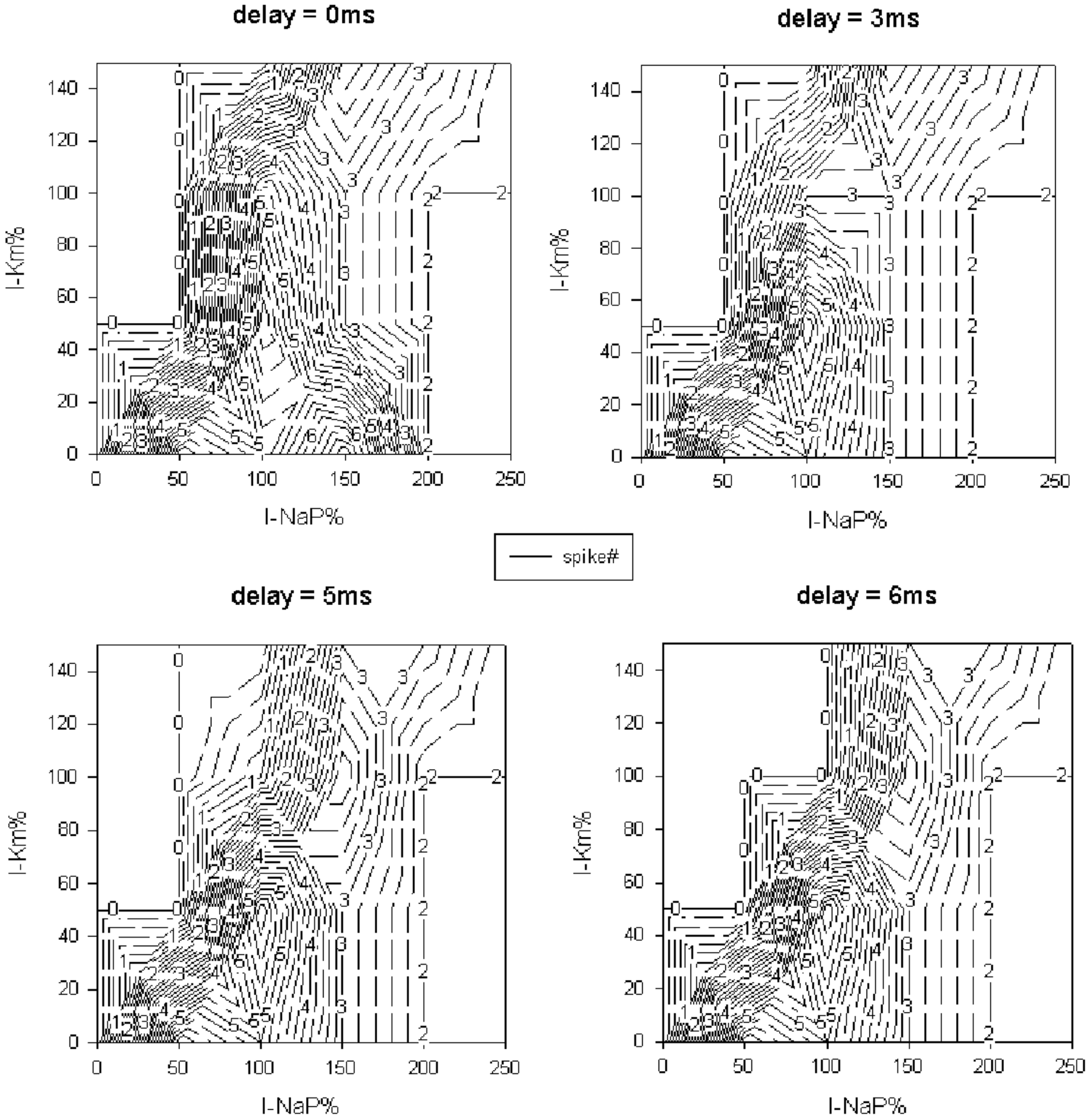
delay = 0ms
delay = 3ms
delay = 5ms
delay = 6ms
I-Km%
I-NaP%
0
20
40
60
80
100
120
140
0
50
100
150
200
250
spike#

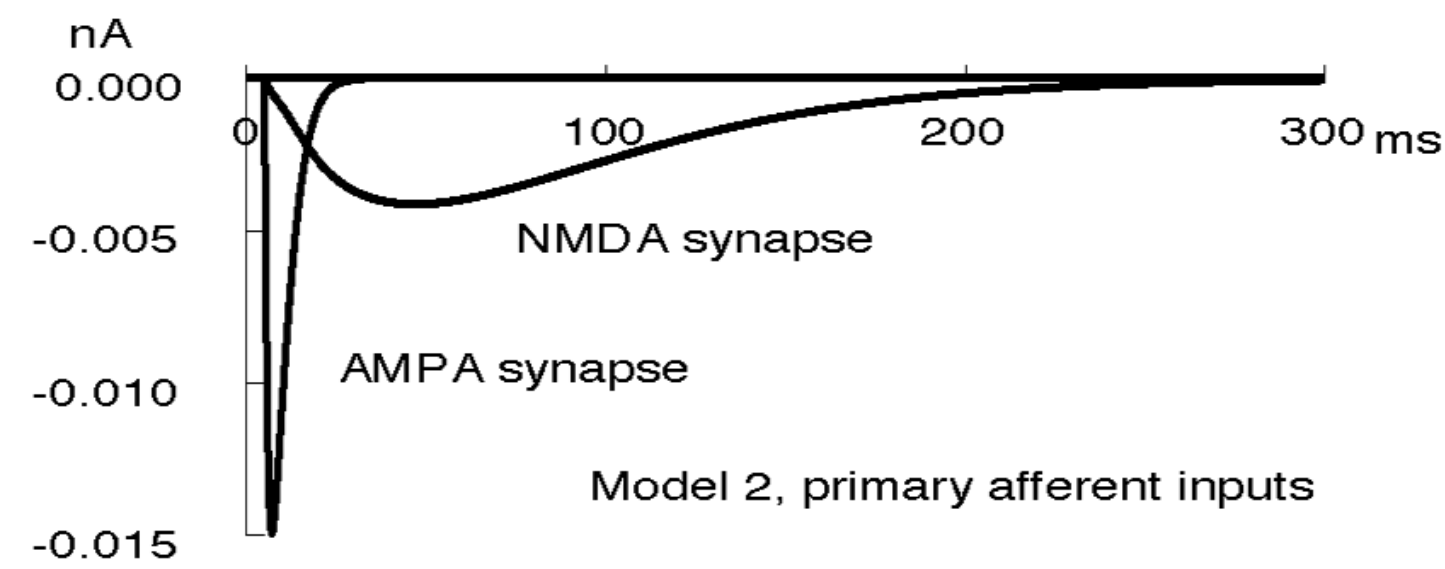
nA
0.000
-0.005
-0.010
-0.015
0
100
200
300 ms
NMDA synapse
AMPA synapse
Model 2, primary afferent inputs

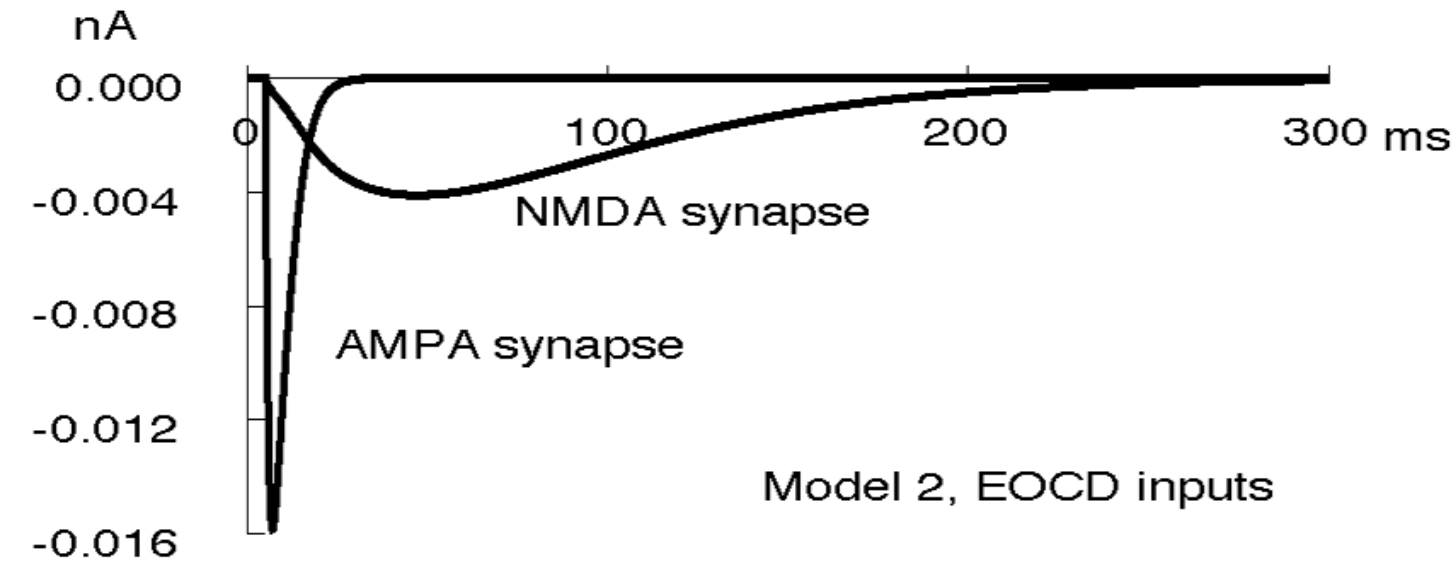
nA
0.000
-0.004
-0.008
-0.012
-0.016
0
100
200
300 ms
NMDA synapse
AMPA synapse
Model 2, EOCD inputs

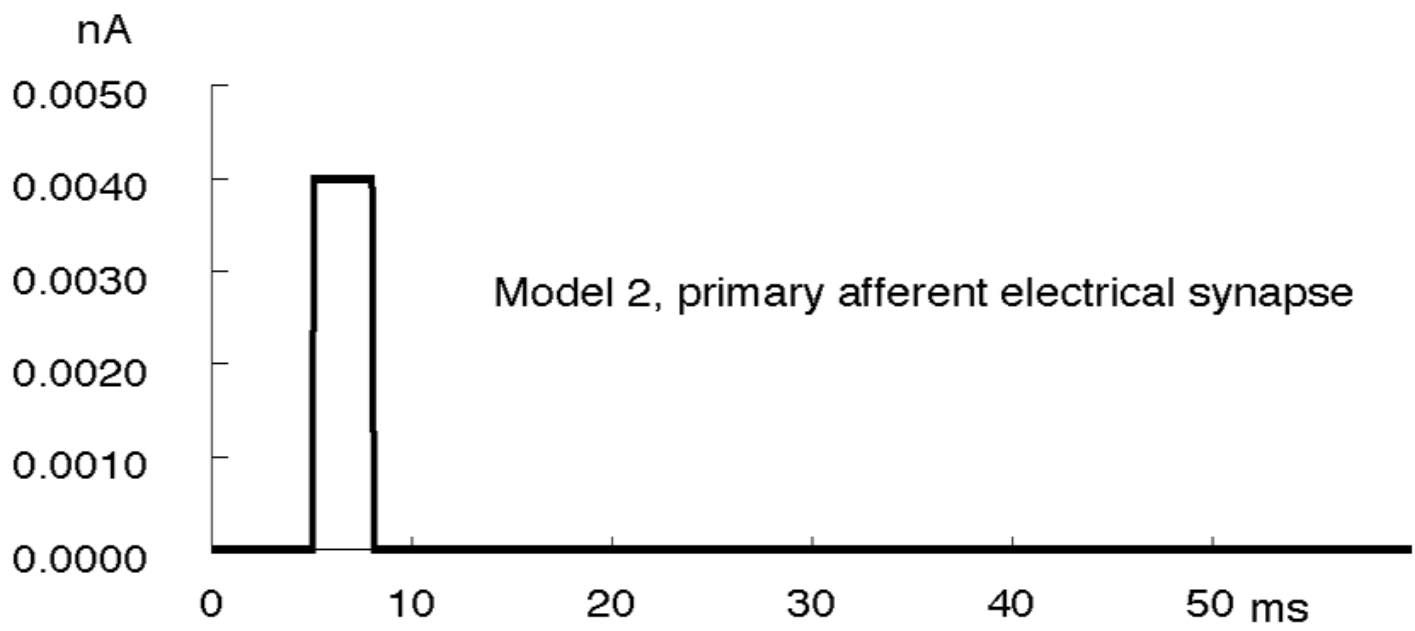
nA
0.0050
0.0040
0.0030
0.0020
0.0010
0.0000
0
10
20
30
40
50 ms
Model 2, primary afferent electrical synapse

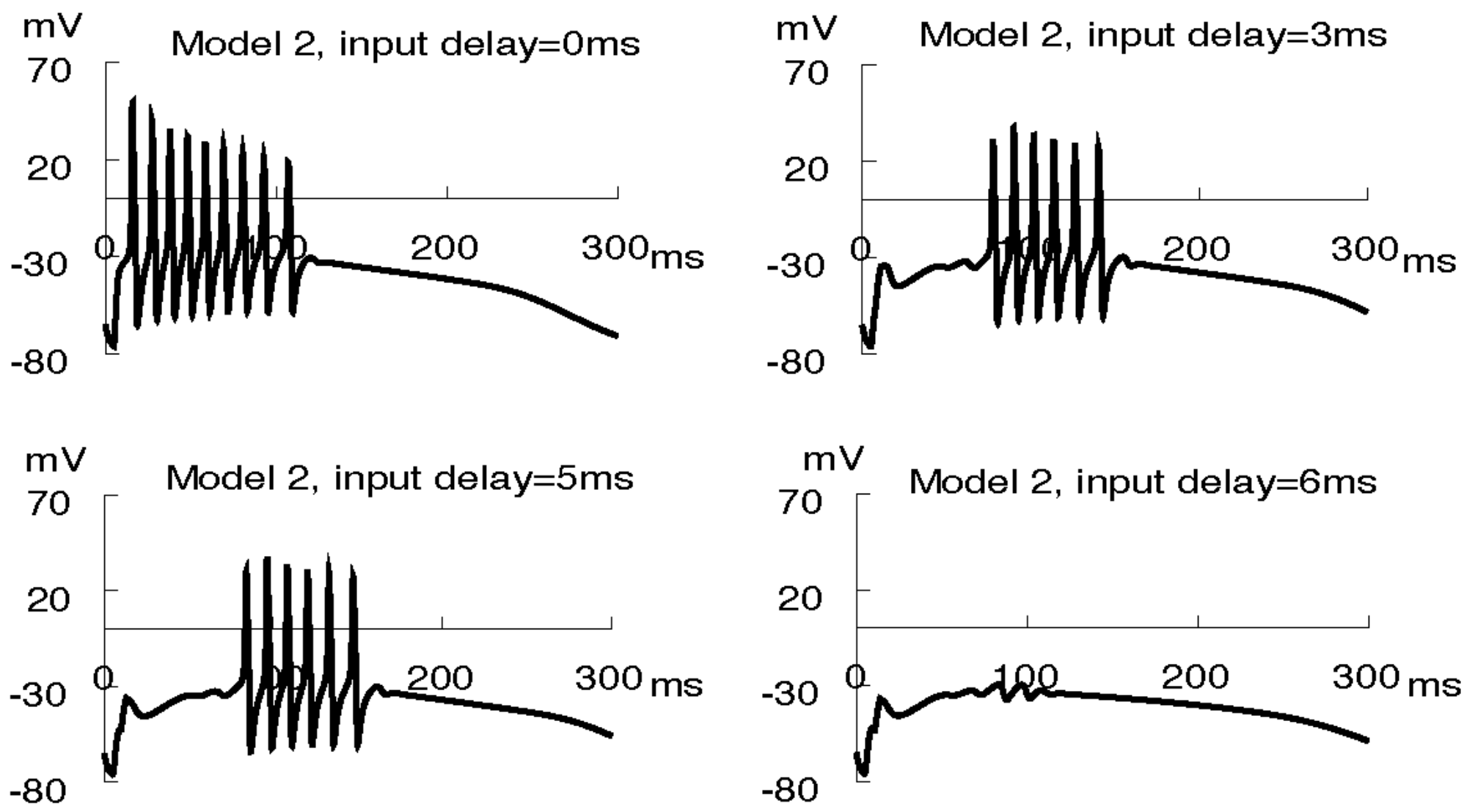
mV
Model 2, input delay=0ms
70
20
-30
-80
0
200
300
ms
mV
Model 2, input delay=3ms
70
20
-30
-80
0
200
300
ms
mV
Model 2, input delay=5ms
70
20
-30
-80
0
200
300
ms
mV
Model 2, input delay=6ms
70
20
-30
-80
0
100
200
300
ms

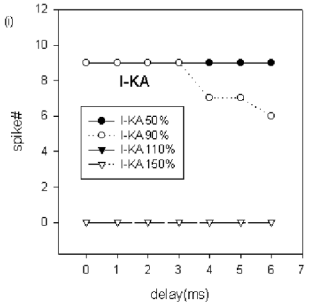
(i)
I-KA
I-KA 50%
I-KA 90%
I-KA 110%
I-KA 150%
spike#
delay(ms)

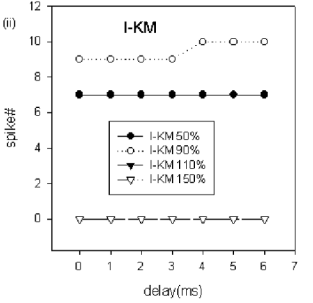
(ii)
I-KM
I-KM 50%
I-KM 90%
I-KM 110%
I-KM 150%
spike#
delay(ms)

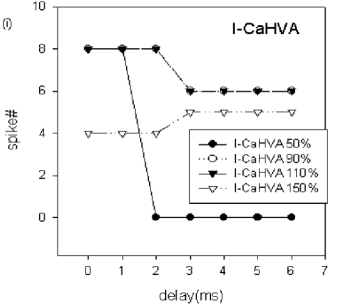
(i)
I-CaHVA
I-CaHVA 50%
I-CaHVA 90%
I-CaHVA 110%
I-CaHVA 150%
spike#
delay(ms)

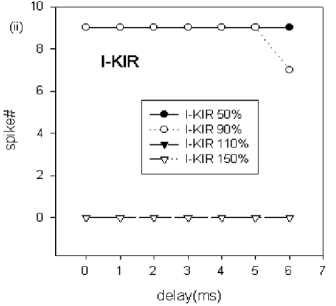
(ii)
I-KIR
I-KIR 50%
I-KIR 90%
I-KIR 110%
I-KIR 150%
spike#
delay(ms)

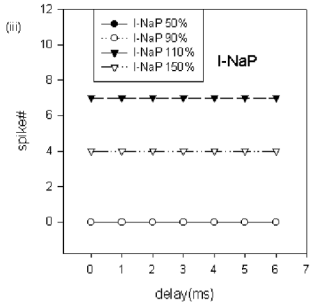
(iii)
I-NaP
I-NaP 50%
I-NaP 90%
I-NaP 110%
I-NaP 150%
spike#
delay(ms)

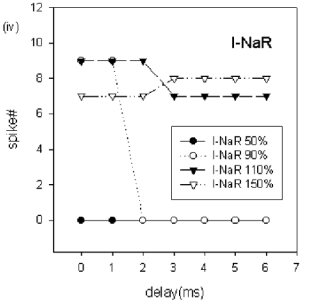
(iv)
I-NaR
I-NaR 50%
I-NaR 90%
I-NaR 110%
I-NaR 150%
spike#
delay(ms)

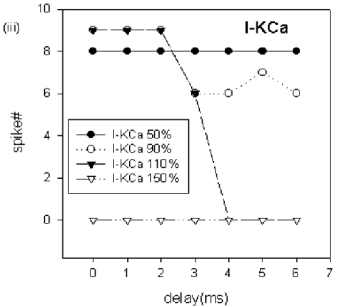
(iii)
I-KCa
I-KCa 50%
I-KCa 90%
I-KCa 110%
I-KCa 150%
spike#
delay(ms)

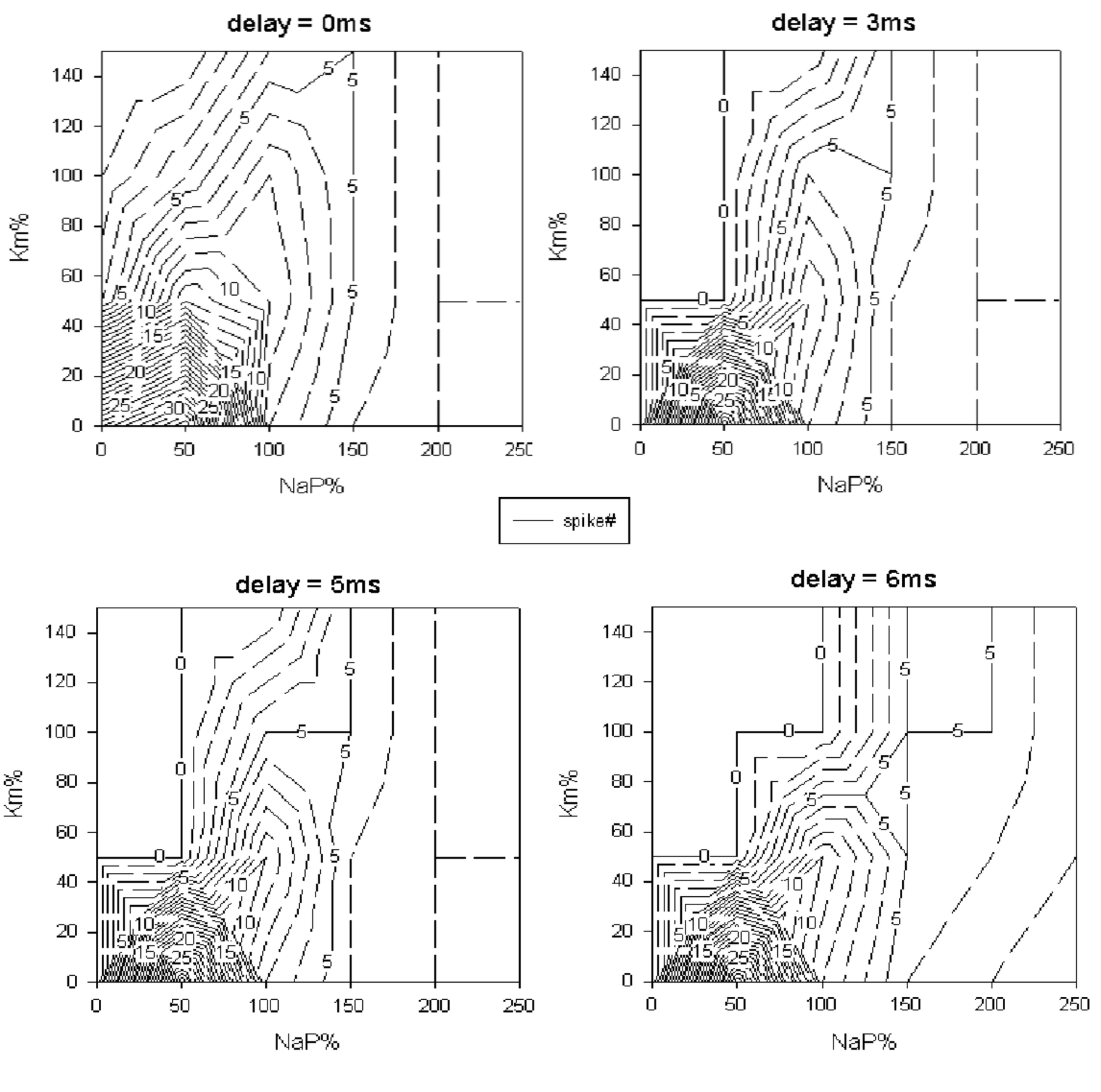
delay = 0ms
delay = 3ms
delay = 5ms
delay = 6ms
Km%
NaP%
spike#